DESIGN AND DEVELOPMENT OF METAL-POLYMER FILM SYSTEMS FOR FLEXIBLE ELECTRODES USED IN CORTICAL MAPPING IN RATS

By

JOHN DAVID YEAGER

A thesis submitted in partial fulfillment of
the requirements for the degree of

MASTER OF SCIENCE IN MATERIALS SCIENCE AND ENGINEERING

WASHINGTON STATE UNIVERSITY
School of Mechanical and Materials Engineering

AUGUST 2008

To the Faculty of Washington State University:

The members of the Committee appointed to examine the thesis of JOHN DAVID YEAGER find it satisfactory and recommend that it be accepted.

_____
Chair

_____

_____

_____

ACKNOWLEDGEMENTS

I would first like to thank Dr. Bahr for his support and guidance during this project. Your keen insight and endless knowledge were constant sources of inspiration for my research, while your tireless work ethic and accommodating nature showed me how to be a professional in every sense of the word. I am fortunate to have such an advisor. I would also like to thank Dr. Rector for his oversight and direction, keeping the project focused and practical when I felt over my head in the research. To my other committee members, Dr. Field and Dr. C. Richards, thank you for your assistance in so many areas above and beyond the reach of this project. Additionally, Dr. John Balk provided the tantalum for part of this study, and the financial support from the W.M. Keck Foundation and the National Institute of Mental Heath under grant numbers MH60263 and MH71830 was greatly appreciated

I would also like to thank the many students who shared their knowledge and time with me. I must first thank Brian Hollenberg, though I never met him, for laying the groundwork for the flexible electrode project. I am also grateful to Molly Kennedy for training me on the four point bend tester, as well as guidance with technical writing. Derrick Phillips and Dr. Manuel Rojas performed many of the electrode implantations, and Derrick in particular has been helpful with statistical analysis and cortical recordings. Numerous graduate students gave advice on MEMS techniques and shared their clean room expertise, and I would like to especially thank Leland Weiss and John Youngsman.

My deepest thanks, however, are reserved for my wife Adria. Your love and support have been my foundation, and I could not have done this without you.

DESIGN AND DEVELOPMENT OF METAL-POLYMER FILM SYSTEMS FOR FLEXIBLE ELECTRODES USED IN CORTICAL MAPPING IN RATS

Abstract

by John David Yeager, M.S.
Washington State University
August 2008

Chair: David F. Bahr

A flexible electrode array for chronic neural implantation in rats has been developed and characterized. Using MEMS techniques, a 64 channel gold on Kapton array was fabricated and tested for electrical and mechanical durability. Principal problems with electrode arrays from previous designs included gold delamination at low strains, relatively low (80%) yield of working channels per array, and proven biocompatibility only for short implantation times. Optimization of fabrication techniques resulted in 95% yield per average array. Using four point bend testing, the effect of a variety of adhesion-promoting treatments were tested. Oxygen plasma etching prior to gold deposition was quantitatively shown to increase the adhesion of gold to Kapton, and use of titanium or a titanium-tungsten alloy interlayer between the gold and Kapton also had significant effect on improving the durability of the device. Gold-Kapton systems with and without these pre-treatments were immersed in 60°C Ringers Solution for a period of 10 weeks to evaluate polymer swelling. The adhesion layers proved to resist failure for at least 10 weeks, while samples without such layers failed at 4 weeks. Implanted electrodes were tested for cortical signal recording in awake rats, and gave meaningful data for at least 80 days.

TABLE OF CONTENTS

LIST OF TABLES

LIST OF FIGURES

CHAPTER 1

INTRODUCTION TO ELECTRODE DESIGN FOR IMPLANTATION

This chapter presents an overview of the field of implantable electrode arrays, their uses and their limitations.

Chapter 1.1 Motivation

The goal of this project was to design a testing method for evaluating the mechanical durability of short-term implantable electrode arrays in rats, and to then use the results from the characterization studies to create a device which could be chronically implanted. The testing method would ideally have application to the field of flexible electronics in general, offering a more quantitative evaluation of device robustness than conventional methods. The improved electrode arrays would be implanted for time periods ranging from three weeks to several years, and have the capability to maintain full capacity within the device itself as well as to avoid tissue irritation over time. The finished device must therefore be capable of surviving several percent strain, induced during implantation, as well as being completely biocompatible. The device also must resist corrosion so as to maintain electrical conductivity over a number of weeks despite a hot, humid, and ion-containing implantation environment.

Chapter 1.2 Literature Review Of Current Implantable Electrodes

Many modern electronic technologies are incorporating flexible substrates in order to increase effectiveness and reliability over a wide range of conditions.

Microelectronic devices which utilize polymers coated with thin films are already being developed for such uses as electronic paper[1], computer displays[2], and smart textiles[3]. The properties of flexible electronics also make them a viable option for small, implantable electrodes for recording brain signals.[4] Adams et al fabricated flexible electrodes and implanted them in frogs to establish a direct connection between nerves in the retina and an analytical computer.[5] They used a metal – polymer system wherein gold is deposited onto either a polyimide or polydimethylsiloxane (PDMS). Their system has successfully recorded electrical response to visual signals. Kitzmiller et al. tested two different types of electrodes for cortical studies in pigs, finding that a gold – polyimide system outperformed a platinum – PDMS system in both durability and electrode density.[6] They further found that human culture cells showed no adverse reaction to the gold – polyimide electrode, indicating that direct application of the electrode technology to human study was possible.

In rats, the recording of brain signals is of great interest. The whiskers on the facial mystacial pad exhibit high levels of tactile information gathering ability. The rat uses the whiskers to locate and distinguish the surrounding environment.[7] The efficiency and resolution of the tactile information is much greater than human fingertips can provide.[8] The whiskers have been shown to directly correlate with the primary somatosensory cortex in the brain.[9] However, much study remains to be done concerning the specific mechanism by which the brain interprets and processes the signals.[10]

Several different techniques exist for recording brain signals in rats, depending on the type of measurement desired. Direct implantation of microwires in mammals has proven exceptionally useful for recording signals from individual neurons.[11] The

drawback of the microwire technique for measuring brain signals is that it requires penetration of brain tissue and removal of large areas of the skull.[12] For chronic studies, the tissue response to wire electrodes can lead to experimental difficulties from mechanical trauma,[13] long term inflammation,[14] and the so-called "glial scar" formation.[15] A comprehensive review on wire electrode implantation issues is given by Polikov et al.[16]

In addition to brain tissue response, simply implanting the electrode may necessitate the removal of large areas of the skull.[17] The trauma induced by the measurement requires an induced coma during recording and subject termination afterwards. Flexible electrodes ideally would minimize trauma to the brain by requiring smaller amounts of skin and bone to be removed in order for implantation to be successful. In addition, the avoidance of tissue trauma should allow for cognizant subject observation. Thin, flexible electrodes have successfully used to penetrate through small slits in the skull and record cortical signals, removing the need to penetrate tissue as well as reducing overall trauma.[18,19] The loss of penetration depth does not adversely affect the amount of useful information gathered. In rats, neural firing in the primary somatosensory cortex directly correlates with whisker stimulation.[9] Similar features appear in the auditory cortex, and since population action potential and excitatory post synaptic potentials can be recorded directly from the cortical surface,[17] it is not necessary to penetrate, and therefore damage the tissue in order to gather meaningful recordings that can be correlated to external stimuli.

Insight into the duration, response time and intensity of these signals may shed light on the mechanism by which the brain interprets external stimuli.[10] Long term

observation should be possible using these electrodes, providing that they have long term durability and that brain will not lose functionality over the course of the study. Therefore, it is imperative that the arrays are mechanically durable and completely biocompatible.

Chapter 1.3 Flexible Electrode Arrays For Implantation In Rats

Implantable flexible electrode arrays for cortical recording using biocompatible materials have previously been developed at Washington State University.[18] Due to the verification of short term implantation success from studies in other animals, a gold – polyimide system was chosen for the arrays. Gold is inert and simple to pattern using standard microelectronics processing methods, and is the most cost-effective metal which satisfies both low impedance and biocompatibility requirements. The additional benefit of simple photolithographic patterning techniques allowed for efficient electrode design. The capabilities of the patterning process for gold exceed the requirements in this case, meaning that higher density electrodes could be produced if the situation arises.

The polyimide chosen for the arrays was Kapton, a polymer with high thermal stability suitable for fabrication procedures. Polyimides have been used successfully in flexible active biomedical implants, showing no reactivity with tissue or bodily fluid.[20] Some varieties of Kapton have shown relatively large water absorption, swelling approximately 2%.[21] This would cause strain at the metal-polymer interface. In addition to swelling strains, sodium cations from the brain fluid can diffuse preferentially into and along the metal-polymer interface rather than through either material, potentially resulting in blister formation and delamination of the film.[22,23] For a sufficiently weak

interface, the strain of implantation and processing may cause delamination regardless of ion accumulation. However, some polyimides with lower water absorption, around 0.5%, have been successfully used for implantable electrodes.[24]

In an earlier study, gold was used for the conductive film for electrode implantation, and an SU-8 epoxy coating was utilized to electrically isolate the gold electrodes as well as to protect them from external damage.[18] These arrays were successful for short-term study of acute rats, but the durability of the arrays may be a concern for chronic long-term implantation. Specifically, experiments on the electrode system indicated that the gold might delaminate from the Kapton at approximately 1% strain; a level that could easily occur during the implantation. Additionally, no consideration of the long-term durability of the electrode in vivo was made in this previous study.

A few other problems arose when fabricating the electrode arrays designed for short-term implantation. The fabrication of the electrode included heat treating steps which caused the finished array to curl. This curling caused some difficulties during implantation, and the subsequent imposed planarization by the surgeon causes strain at the polymer – metal interface, which will allow for easier delamination and failure over long-term exposure in a hot and humid environment. In addition, the Kapton as-fabricated had very sharp edges which could damage the brain during implantation. Finally, the alignment jig which Hollenberg et al. used to stabilize the array and connect it to a computer was bulky and unsuitable for an unconstrained rat to carry for awake recordings. The jig itself also placed enough pressure on the array that disassembly tended to delaminate the gold from the Kapton, preventing reuse.

Chapter 1.4 Research Objectives

The goal of this thesis was to improve upon the electrode array designed by Hollenberg et al. The finished device needed to be perfectly planar, connect simply and repetitively with a computer, have rounded edges to avoid cutting the brain during implantation, and be mechanically and chemically robust so as to facilitate long-term implantation. Such improvements needed to be made without changing the core requirements of the array – low impedance for good signal measurement, biocompatible with the rat's brain, flexible enough to slip through a slit in the skull but stiff enough to be handled by a surgeon, and simple enough in geometry and pattern design to allow for high spatial resolution.

In order to assess the mechanical durability of the device, a test method needed to be designed for measuring the strength of the gold – polymer adhesion. The test should be quantitative enough in nature so as to provide insight into the fundamentals of adhesion of a thin film on a compliant substrate. This would allow for application into the wide-ranging field of flexible electronics. Ideally, the gold – polymer adhesion would be characterized and then the effect of various physical or chemical pre-treatments could be assessed. Four point bend testing has been shown to be an ideal method for determining thin film adhesion energy,[25] and was chosen as the characterizing test method for the film systems used for the electrodes.

References

[1] Y. Chen, J. Au, P. Kazlas, A. Ritenour, H. Gates and M. McCreary. Electronic paper: Flexible active-matrix electronic ink display. Nature 423, 136 (2003)

[2] D. Kim, C. Yu, Y. Lim, J. Na, and S. Le. Mechanical stability of a flexible ferroelectric liquid crystal display with a periodic array of columnar spacers. Applied Physics Letters 87 (2005)

[3] A. Yadav, K.P. Pipe, and M. Shtein. Fiber-based flexible thermoelectric power generator. Journal of Power Sources 175 (2008) 909–13

[4] S. Takeuchi, T. Suzuki, K. Mabuchi, and H. Fujita, 3D flexible multichannel neural probe array. Journal of Micromechanics and Microengineering 14 (2004) 104–7

[5] C. Adams, K. Mathieson, D. Gunning, W. Cunningham, M. Rahman, J.D. Morrison, and M.L. Prydderch. Development of flexible arrays for in vivo neuronal recording and stimulation. Nuclear Instruments and Methods in Physics Research A 546 (2005) 154 –9

[6] J.P. Kitzmiller, D.J. Hansford, L.D. Fortin, K.H. Obrietan, V.K. Bergdall, and D.Q. Beversdorf. Micro-field evoked potentials recorded from the porcine sub-dural cortical surface utilizing a microelectrode array. Journal of Neuroscience Methods 162 (2007) 155–61

[7] W.I. Welker. Analysis of sniffing of the albino rat. Behaviour 22 (1964) 223–44.

[8] G.E. Carvell and D.J. Simons. Biometric analyses of vibrissal tactile discrimination in the rat. Journal of Neuroscience Methods 10 (1990) 2638–48.

[9] T.A. Woolsey and H. Van der Loos. The structural organization of layer IV in the somatosensory region (SI) of mouse cerebral cortex. Brain Research 17 (1970) 205–42.

[10] T. Prigg, D. Goldreich, G. Carvell, and D.J. Simons, Texture discrimination and unit recordings in the rat whisker/barrel system, Physiology & Behavior 77 (2002) 671-5

[11] F. Strumwasser. Long-Term Recording from Single Neurons in Brain of Unrestrained Mammals. Science 127 (1958) 469-70.

[12] C.S. Bjornsson, S.J. Oh, Y.A. Al-Kofahi, Y.J. Lim, K.L. Smith, J.N. Turner, S. De, B. Roysam, W. Shain and S.J. Kim. Effects of insertion conditions on tissue strain and vascular damage during neuroprosthetic device insertion. Journal of Neural Engineering 3 (2006) 196-207

[13] S. Schmidt, K. Horch, and R. Normann. Biocompatibility of silicon-based electrode arrays implanted in feline cortical tissue. Journal of Biomedical Materials Research 27, 11 (1993) 1393-99

[14] D.H. Szarowski, M.D. Andersen, S. Retterer, A.J. Spence, M. Isaacson, H.G. Craighead, J.N. Turner, and W. Shain. Brain responses to micro-machined silicon devices. Brain Research 983 (2003) 23–35

[15] E.M. Maynard, E. Fernandez, and R.A. Normann. A technique to prevent dural adhesions to chronically implanted microelectrode arrays. Journal of Neuroscience Methods 97 (2000) 93–101

[16] V.S. Polikov, P.A. Tresco, and W.M. Reichert. Response of brain tissue to chronically implanted neural electrode. Journal of Neuroscience Methods 148 (2005) 1–18

[17] M.S. Jones and D.S. Barth. Spatiotemporal organization of fast (>200Hz) electrical oscillations in rat vibrissa/barrel cortex. Journal of Neurophysiology 82, 3 (1999) 1599–609

[18] B.A. Hollenberg, C.D. Richards, R. Richards, D.F. Bahr, and D.M. Rector. A MEMS Fabricated Flexible Electrode Array for Recording Surface Field Potentials. Journal of Neuroscience Methods 153, 1 (2006) 147-53

[19] K.C. Cheung, P. Renaud, H.Tanila, and K. Djupsund. Flexible polyimide microelectrode array for in vivo recordings and current source density analysis. Biosensors and Bioelectronics 22 (2007) 1783–90.

[20] T. Stieglitz and J.U. Meyer. Implantable Microsystems: Polyimide-Based Neuroprostheses for Interfacing Nerves. Medical Device Technology 10, 6 (1999) 28-30

[21] J.F Hetke, K. Najafi, and K.D.Wise. Flexible Miniature Cables for Long-term Connection to Implantable Sensors. Sensors and Actuators A 21(1990) 999-1002

[22] J. Pommersheim, T. Nguyen, Z. Zhang, and C. Lin. Cation Diffusion at the Polymer Coating / Metal Interface, Journal of Adhesion Science and Technology 9 (1995) 935-51

[23]A. Leng, H. Streckel, M. Stratmann. The Delamination of Polymeric Coatings from Steel. Part 1: Calibration of the Kelvinprobe and Basic Delamination Mechanism. Corrosion Science 41 (1999) 547-78

[24] T. Stieglitz, H.H. Ruf, M. Gross, M. Schuettler, J.U. Meyer. A biohybrid system to interface peripheral nerves after traumatic lesions: design of a high channel sieve electrode. Biosensors and Bioelectronics 17 (2002) 685-96.

[25] M.P. Hughey, D.J. Morris, R.F. Cook, S.P. Bozeman , B.L. Kelly, S.L.N. Chakravarty, D.P. Harkens, and L.C. Stearns. Four-point bend adhesion measurements of copper and permalloy systems. Engineering Fracture Mechanics 71 (2004) 245-61

CHAPTER 2

LITERATURE OVERVIEW OF FOUR POINT BEND TESTING AS A METHOD FOR CHARACTERIZING FILM ADHESION

This chapter summarizes a review of the literature about four point bend testing as it relates to characterizing thin film devices. The test is simple to perform, the samples are easy to fabricate, and the overall time invested in determining device reliability is relatively short. Furthermore, the mechanics of the method are well understood for the purely elastic case, and the steady-state crack propagation allows for precise adhesion energy calculation. The literature review presented in this chapter will focus on the mechanics of failure in the four point bend test system and the direct application of the test to multilayer structures. Mixed mode delamination will be discussed, and the effect of phase angle on the measured adhesion will be explained.

Chapter 2.1 Four Point Bend Testing of Elastic Multilayer Structures

Several researchers have found small-scale four point bend testing to be a useful method of isolating delamination energy and quantifying adhesion of a film to a substrate through a linear elastic fracture mechanics (LEFM) based approach[1,2,3,4,5]. Figure 2.1 shows a typical four point testing arrangement for adhesion testing.

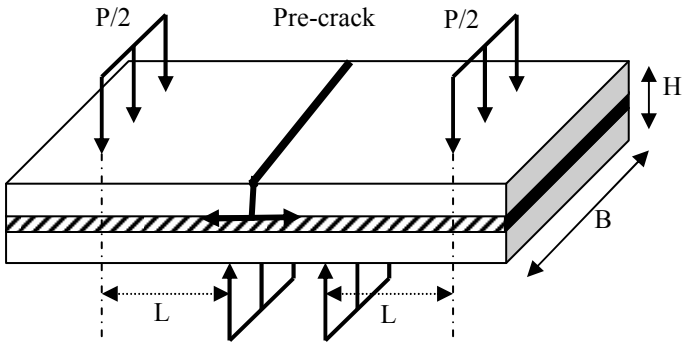

Figure 2.1 A four point bend test specimen consisting of a thin film stack sandwiched between two elastic beams, showing probable crack path.

Typical testing geometry consists of two elastic layers (silicon or glass are common choices) that sandwich a set of film systems. The top of the composite beam is notched with a diamond scribe to initiate a crack site. The notch must be aligned in the center of the four point testing apparatus so as to have a symmetrical moment about the crack. The load is applied and displacement is measured as the crack propagates. The crack moves vertically through the top elastic layer until it reaches the interfacial layer. The crack then may continue its vertical descent or it may propagate laterally as depicted in the figure. A typical load vs. displacement curve is shown in Figure 2.2. The strength of adhesion between the film and the substrate controls the crack direction, as the crack will travel along the path of least resistance[1].

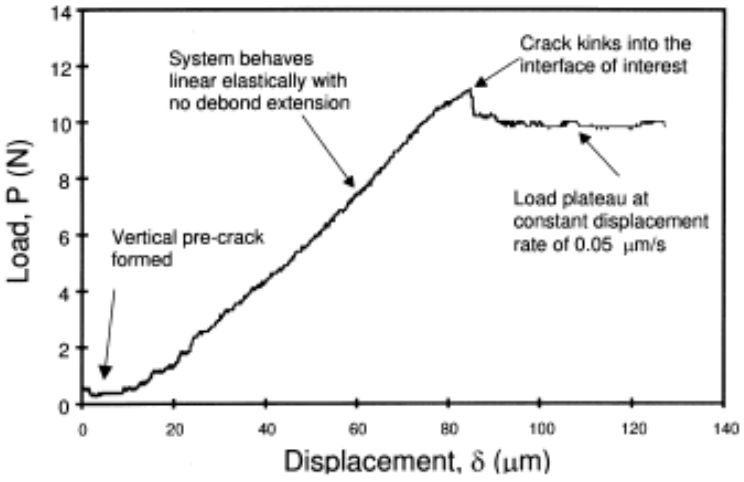

Figure 2.2 Typical load - displacement curve for a silicon-constrained sandwich specimen[1]

If the crack propagates laterally along an interface of the specimen, the load – displacement curve shows a distinctive plateau, which can depend on the testing conditions[2]. This plateau occurs when the crack is moving laterally, e.g. along an interface. The load at this plateau can then be used in Equation 1 to find the strain energy release rate, G, which characterizes the toughness of the interface. In the purely elastic case, the energy release rate (per unit area) at delamination is given by

$$G = g\frac{L^2P^2(1-\nu^2)}{EB^2H^3} \qquad (1)$$

where L is distance between an inner and outer pin, P is the applied load at the plateau, ν is Poisson's ratio, E is the modulus of the elastic substrate, and B and H are respectively the width and height of the specimen, with reference to Figure 2.1. The geometric factor, g, which depends on elastic substrate thickness, is 21 / 16, or 1.3125, when the elastic substrates have the same thickness, as seen in other sandwich specimen reports[1]. This energy release rate value is equal to the crack extension energy during crack

propagation[3]. Thus a measure of the energy release rate can be found for delamination in elastic systems, giving a value for the adhesion strength of the interface.

Chapter 2.2 Accounting for Plasticity in Sandwich Specimens

In general, the elastic beams shown in the figure are also the substrates for the films of interest. Therefore, it should be noted that the bend tests have so far only proven suitable for perfectly elastic systems, since plastic deformation may affect the measurement. Other plastic effects such as creep or stress relaxation may occur in these systems, resulting in calculated toughness values somewhat lower than the true toughness. Liu et al. summarize a body of work on the subject by separating the measured, or extrinsic, steady state (SS) toughness into interfacial separation and inelastic deformation quantities,

$$\Gamma_{SS} = \Gamma_0 + \Gamma_P \qquad (2)$$

where Γ_0 is the intrinsic adhesion energy, related to the materials at the interface, and Γ_P is the plastic dissipation energy, which depends on mechanical properties as well as the specimen geometry.[6] They then undertook computational studies to determine the effect of various parameters on the measured and intrinsic toughness. One important result was that four point bend testing samples with a ductile film thickness on the order of 10% of the plastic zone size (ahead of the crack tip) essentially eliminated Γ_P, so that $\Gamma_{SS} \approx \Gamma_0$. A relationship is given for determining the true work of adhesion based on normalized film thickness, and the resulting graph is shown in Figure 2.3. The film thickness here is normalized by the plastic zone size, R_0, which is the region ahead of the crack tip which experiences plastic deformation due to high stresses. The general relationship between

film thickness and measured toughness given by Liu is that increases in thickness of the ductile film lead to increases in Γ_{SS}. This has been experimentally verified elsewhere.[7]

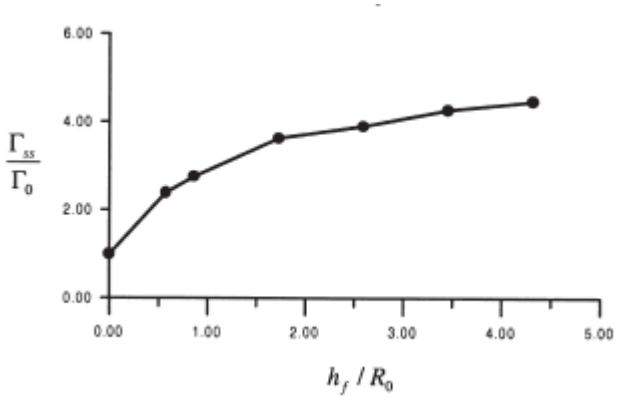

Figure 2.3 Effect of film thickness to plastic zone size ratio on measured adhesion values[6]

In the gold-Kapton system considered for this thesis, the ability to reach a completely elastic measurement was limited somewhat by the necessity of using 25μm Kapton. However, some valid comparisons may still be made to the idealized system from Liu et al. Affixing the plastic layer to a brittle elastic material should at least yield relative, if not absolute, information about the interfacial toughness of the system. Additionally, using elastic plates will constrain subsequent plasticity in the interface. This constrained plasticity allows for valid usage of the linear elastic approach in some systems.[8]

Chapter 2.3 Effect of Phase Angle on Calculated Toughness

In addition to the convenience of measuring delamination at any interface of interest, the four point bend test method has the advantage of sampling the material in a way which mimics stresses that the film will undergo during actual use. The test does this

by providing both shear and normal stresses during delamination of the film.[9] The phase angle, Ψ, represents the amount of mixed-mode stress is present in the system, and is defined by the complex stress intensity factor (K) in Equation 3.[10]

$$K = \mathrm{Re}(K) + i\,\mathrm{Im}(K) \equiv (K)e^{i\Psi} \qquad (3)$$

For a system with two identical elastic substrates, the overall value of Ψ is 41.6 degrees.[6,10] However, the phase angle may change slightly at the tip of the crack during delamination of the film from the substrate. This modified tip relationship is given in Equation 4 as

$$\Psi_{tip} = \Psi + \omega + \varepsilon \ln H \qquad (4)$$

where ω is an angle determined by the materials adjoining the interface[7], ε is related to a plain strain parameter, in turn related to the shear moduli and Poisson's ratios of the materials, and H is the film thickness.[10] Thus the amount of mixed mode behavior in the four point bend test can be determined simply by film thickness and material constants. Specimen geometry alterations will also affect the phase angle. Modification of Equations 3 and 4 yield the following expression

$$\Psi = \tan^{-1}\left[\frac{\mathrm{Im}(Kl^{i\varepsilon})}{\mathrm{Re}(Kl^{i\varepsilon})}\right] \qquad (5)$$

where *l* is a reference length specific to specimen geometry and all other terms have been previously defined.[11] This reference length is not a material-specific parameter; it only depends on test design parameters such as substrate thickness or crack length at failure.

It is often convenient to relate the calculated fracture toughness from the four point bend test to values from other test methods. One important way to do this is to find the Mode I fracture toughness, K_{IC}, of the interface. This is given by

$$\Gamma_0 = \frac{\Gamma_{(\Psi)}}{1+\tan^2\left[\Psi(1-\lambda)\right]} \qquad (6)$$

where Γ_0 is equivalent to K_{IC}, $\Gamma_{(\Psi)}$ is the measured toughness at some phase angle, and λ is a dimensionless adjustable parameter between 0 and 1.[11] A value of 1 for λ means that the sandwich specimen is perfectly brittle, with equal contribution from Mode I and II, while λ of 0 means pure Mode I fracture. λ is often taken to be 0.3 for substrates with similar elastic modulus. Thus the Mode I fracture toughness can be found for a measured toughness at any phase angle.

The effect of a thick stack of interlayers on phase angle is not currently known. However, the undetermined phase angle should still remain constant between the loading points, allowing for relative interfacial energy measurements. All of the specimens for this thesis were manufactured and tested in a precise manner, and so it is assumed that they all experience similar fracture events. Calculating the Mode I fracture toughness of the interface is therefore unreliable for the samples described in Chapter 3, but the relative fracture toughness at some phase angle is still valid.

References

[1] R.H. Dauskardt, M. Lane, Q. Ma, and N. Krishna, Adhesion and debonding of multi-layer thin film structures. Engineering Fracture Mechanics 61 (1998) 141-62

[2] M.P. Hughey, D.J. Morris, R.F. Cook, S.P. Bozeman , B.L. Kelly, S.L.N. Chakravarty, D.P. Harkens, and L.C. Stearns. Four-point bend adhesion measurements of copper and permalloy systems. Engineering Fracture Mechanics 71 (2004) 245-61

[3] Z. Huang, Z. Suo, G. Xu, J. He, J.H. Prévost, and N. Sukumar. Initiation and arrest of an interfacial crack in a four-point bend test. Engineering Fracture Mechanics 72 (2005) 2584-601

[4] S. Roham, K. Hardikar, and P. Woytowitz. Stress Analysis of 4-Point Bend Test for Thin Film Adhesion. Materials Research Society Symposium Proceedings 778 (2003)

[5] S. Gandikota, S. Voss, R. Tao, A. Duboust, D. Cong, L. Chen, S. Ramaswami, and D. Carl. Adhesion studies of CVD copper metallization. Microelectronic Engineering 50 (2000) 547-53

[6] P. Liu, L. Cheng, and Y. W. Zhang. Measuring Interface Parameters and Toughness – A Computational Study. Acta Materialia 49 (2001) 817-25

[7] H. F. Wang, W. W Gerberich, and C.J. Skowronek. Fracture Mechanics of Ti/Al_2O_3 Interfaces. Acta Metallurgica et Materialia 41, 8 (1993) 2425-32

[8] Z. Suo, J.W. Hutchinson. On sandwiched test specimens for measuring interface crack toughness. Materials Science & Engineering A 107 (1989) 135-43.

[9] P.G. Charalambides, J. Lund, A.G. Evans and R. M. McMeeking. A test specimen for determining fracture resistance of bimaterial interfaces. Journal of Applied Mechanics 56 (1989) 77-82.

[10] P.G. Charalambides, H.C. Cao, J. Lund and A.G Evans. Development of a test method for measuring the mixed mode fracture resistance of bimaterial interfaces. Mechanics of Materials 8 (1990) 269-83.

[11] J.W. Hutchinson, Z. Suo. Mixed Mode Cracking in Layered Materials. Advances in Applied Mechanics 29 (1992)

CHAPTER 3

EXPERIMENTAL METHODS AND MATERIALS

This chapter describes the standard experimental techniques used for the majority of the studies presented in this thesis. Unless otherwise stated, it is assumed that the methods in this chapter are used for all specimen fabrication. Over the course of the research for this thesis several improvements were made to the electrode fabrication technique. The improvements are reported here, rather than the previous process initially used to make the electrodes. Some advances in the macrofabrication or electrode assembly process will also be reported in this chapter. These modifications were necessary for long-term implantation. The techniques described in this chapter are the current standard for electrode fabrication, four point bend test sample preparation, and characterization studies.

Chapter 3.1 Clean Room Microfabrication of Flexible Electrodes

Hollenberg et al developed a successful electrode array for short term implantation at Washington State University.[1] The array had an 8x8 grid of 150 μm diameter circles which aligned well with the cortical barrels in the female rat cortex, as shown in Figure 3.1.[2]

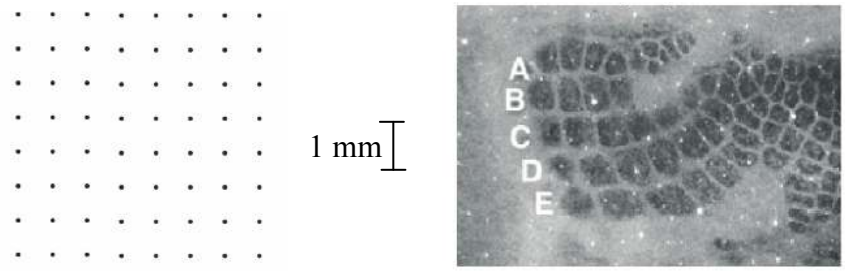

Figure 3.1 Spacing of electrode array compared to cortical barrels, photo from [2]

Each grid point was connected to an external source via a 50 to 150 μm wide trace and connector pad. The trace had to be long enough to reach from inside the skull to at least the top of the head for connection to a computer, which is approximately 20mm. Hollenberg's 22.5 mm long electrode design is shown in Figure 3.2.

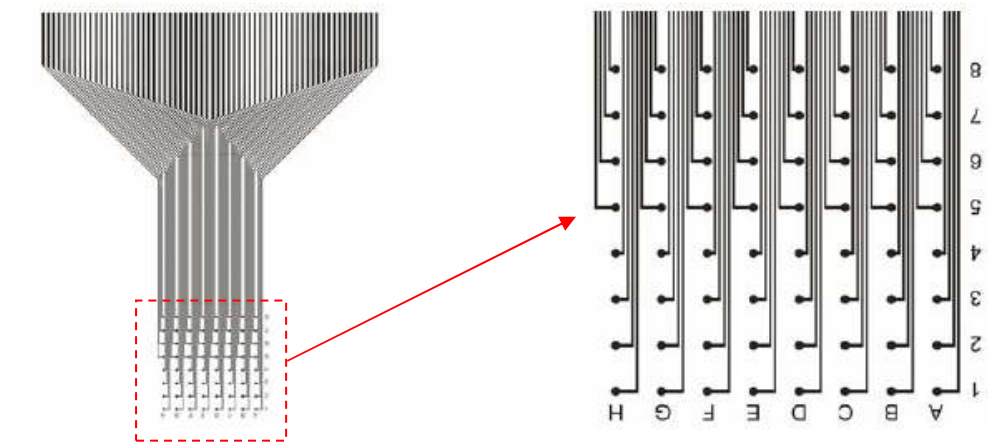

Figure 3.2 Electrode array designed by Hollenberg[1]

This design was used for the initial studies reported in this thesis. Advantages of other designs will be later in this chapter.

The electrode arrays were fabricated in a Class 1000 clean room to minimize contamination. The materials chosen for the flexible array were outlined and justified in Chapter 1.3, but will be reiterated in this section. The flexible substrate chosen was a

polyimide film (Kapton), purchased from DuPont Chemical Corp (Wilmington, DE) in 25μm thick rolls. 25 x 75 x 0.5 mm microscope glass slides were used as handling wafers, as the Kapton was not sturdy enough on its own to withstand processing. The film was cut into a 25 x 75 mm rectangle and secured to a glass slide with Kapton tape (Dupont). The Kapton was then cleaned with a five step cleaning process, sequentially washing with acetone, isopropyl alcohol (IPA), de-ionized water, acetone, and then IPA. The first acetone, IPA and de-ionized water steps were to allow removal of various types of contaminants, and the last steps were to dissolve and remove the liquid from the previous step. After the final IPA washing, the sample was carefully dried with nitrogen gas.

After the five step cleaning process, the sample was placed into a PE-2000 RF Plasma Etching system (South Bay Technology Inc., San Clemente, CA). After evacuation to 50 $x10^{-3}$ torr, oxygen gas was introduced into the chamber at a pressure of approximately 135 $x10^{-3}$ torr. The Kapton was then radio-frequency (RF) oxygen plasma etched at 100 W for three minutes. The etching was done to chemically alter the surface of the polyimide in order to enhance adhesion.[3] The positive effect of the plasma etching is verified and quantified in Chapter 4 of this thesis.

Immediately after etching the Kapton was transferred to a DC Magnetron sputtering system (Edwards Auto 306, Wilmington, MA). The system had two metallic targets, which allow for the deposition of alternating metal layers without breaking vacuum. In all cases a gold target was used for the electrode layer, and various metals and alloys were used as the other target as an adhesion layer. The effect of the adhesion layers on the gold - Kapton interface is quantified in Chapter 5. The sputtering chamber

was then evacuated to a base pressure of less than $1x10^{-6}$ torr. Argon was introduced into the chamber, bringing the process pressure up to $7.5\ x10^{-3}$ torr. The argon was then ionized into a plasma, and after a two minute shield sputtering time to scour the target surface and remove impurities, gold was sputter deposited for 23:12 at 75 W power. The samples were rotated above the targets to deposit uniformly on multiple samples. This sputtering process produced a gold thickness of 300 nm. In the cases where an adhesion layer was utilized, a thin (5 to 10 nm) metal layer was sputtered directly before the gold. The specific recipe depends on the metal used, but in general the processing parameters were similar to the gold, only on the order of one minute rather than 23:12. After sputtering had been completed, the specimens were plasma etched again for three minutes using the process noted above, this time as a routine surface cleaning method. The specimens were then spin-coated with a photoresist (AZ5214, Clariant) for photolithographic patterning. The patterning process is visually represented in Figure 3.3.

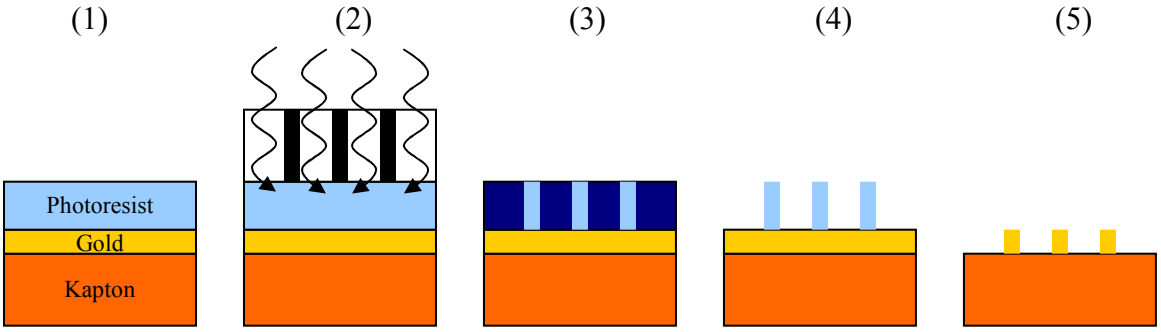

Figure 3.3 Schematic of photolithography process
(1) Photoresist is spin coated onto Au-Kapton.
(2) Patterned mask is placed on sample and exposed to UV light.
(3) This results in regions of differing chemistry in the photoresist.
(4) Immersion in developing solution removes exposed resist.
(5) Immersion in gold etchant removes unprotected gold film, leaving a pattern behind. Cleaning in acetone removes leftover resist.

The samples were placed onto a rotating chuck and held in place by a vacuum. The liquid photoresist was then deposited on top of the gold – Kapton sample with a pipette. Then the sample was spun at 3000 rpm for 30 seconds to achieve the desired photoresist thickness. A soft bake at 110°C removed any remaining solvent from the photoresist. Then a positive photomask pattern (chrome patterned on glass) was placed over the specimen and the whole assembly was exposed to UV light for 45 seconds. The UV radiation chemically alters the exposed portions of the photoresist, resulting in regions susceptible to removal by a developing solution. After exposure, the sample was immersed in AZ400K developing solution (Clariant) for 60 seconds. At this point, the specimen had both regions of exposed gold and of gold covered with the patterned photoresist. The exposed gold was then removed with an iodine based chemical etch (TFA, Transene Company Inc., Danvers, MA), which was performed at room temperature through a liquid immersion process for approximately 60 seconds, leaving only gold in the desired pattern. The remaining photoresist was then washed off with the five step cleaning process described earlier.

After patterning, another routine plasma etch was performed in the same way as the previous etching. Then a thick photoresist (SU-8, Shipley Manufacturing, Marlborough, MA) was spin-coated onto the sample in a similar manner as to the gold patterning photoresist. In this case, the samples were spun at 2000 rpm for 30 seconds, followed by soft baking steps of 1 minute at 65°C and 2 minutes at 95°C. This provided an SU-8 layer at a thickness of approximately 10 μm. This thickness provides a slight stress in the film that balances any stresses that are present in the gold layer, allowing for a finished film that is effectively flat. After the baking steps, a different glass mask was

used to negatively pattern the SU-8 under UV light. This mask allowed for negative photoresist development, meaning that the exposed portions of the SU-8 cross-linked and became chemically resistant, which is the reverse of the process in Figure 3.3. Thus only the dot array for brain contact and the electrode pads for electronic signal measurement were covered by the mask, as shown in Figure 3.4 below.

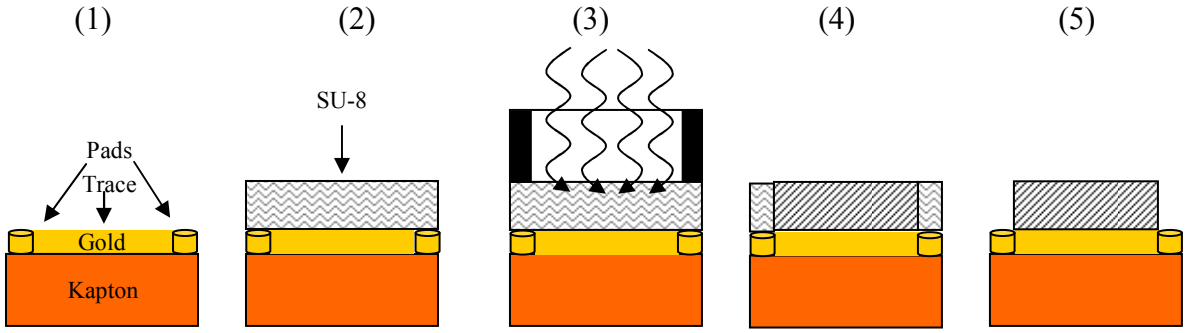

Figure 3.4 Schematic of SU-8 deposition process
(1) The patterned gold is placed in the spin coater
(2) SU-8 is spun onto the gold at a thickness of ~10µm
(3) The SU-8 is exposed to UV light through a chrome mask
(4) Baking and developing reveals areas of differing chemistry
(5) Final rinse and developing cycle allows for exposed gold pads with isolated and protected gold traces

After a post-exposure bake cycle of 2 minutes at 65°C, 3 minutes at 95°C, and 1 minute again at 65°C, the specimen was immersed in SU-8 developer (MicroChem) for three minutes. This hardened the cross-linked areas of the SU-8, and a subsequent five step cleaning process removed the unexposed pattern. Then the samples were baked for a curing cycle at 150°C for ten minutes to finalize the SU-8 pattern. The samples were thus ready for implantation. Figure 3.5 is a micrograph of a portion of the electrode, showing the SU-8 protection and exposed gold for recording cortical signals.

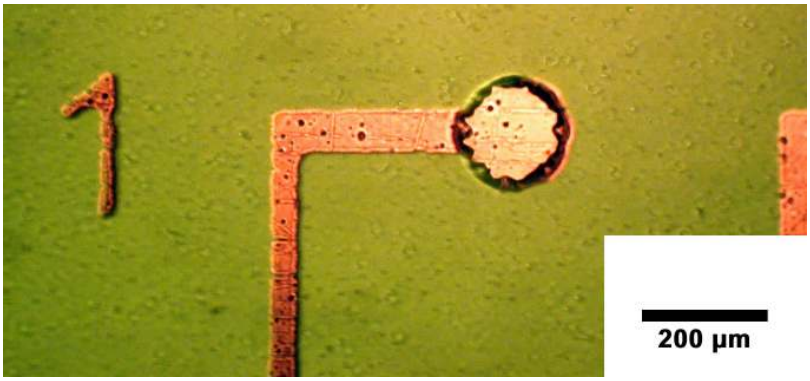

Figure 3.5 A corner of the electrode array, covered with SU-8 except directly over the pad

Chapter 3.2 Shaping the Electrode Array

Once the electrode had been fabricated in the clean room, it needed to be removed from the unused Kapton and the handling wafer. A steel rule die was designed and purchased from Empire Screen Printing (Onalaska, WI) in order to stamp the electrode out of the Kapton sheet. Stamping was chosen as the method for electrode removal based on a number of factors: first, a reliable die would allow for a repeatable final shape which would not change per electrode batch; second, the rule die provided a cutting edge outline of the electrode shape, meaning that no physical contact with the main array was necessary for removal; and third, the rule die cutting edges gradually came to a sharp point, hopefully causing the edge of the stamped electrode to be neat but somewhat rounded. An electron micrograph comparing a stamped Kapton edge to razor and scissor cutting is shown in Figure 3.6.

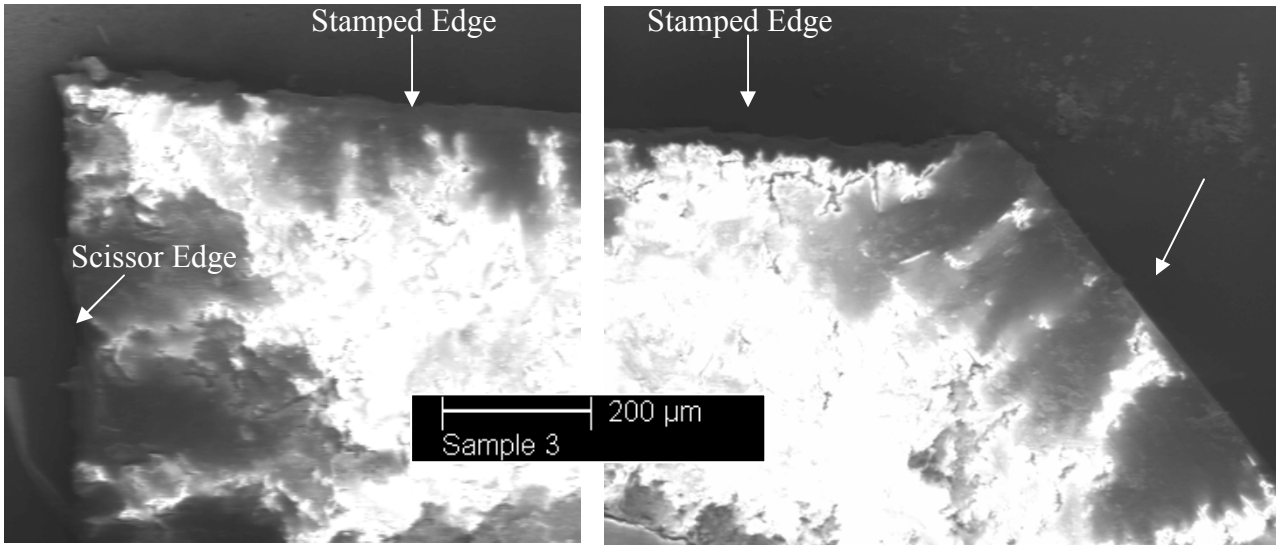

Figure 3.6 Comparison of stamped edges to razor and scissor edges

While it is difficult to take electron micrographs of a non-conductive sample, such as Kapton, the general outline of the edges can be viewed in the figure. While the scissor edge looks somewhat jagged, the stamp edge is relatively clean and precise. The razor definitely produces the sharpest edge, but can deviate from a straight line. Thus, stamping was verified to be a convenient mixture of the two extremes – not too sharp, so as to avoid cutting the brain when implanted, but not too jagged, so as to avoid getting caught on the dura or the skull and ripping the electrode. It should be noted that the stamp purchased for the project was manufactured by a craft supply outlet. It is suspected that a high quality stamp purchased from an industrial supplier would create an even cleaner outline without sharpening the edge too much. The stamping done on all electrode arrays was at 4000psi.

Chapter 3.3 New Electrode Pattern for Chronic Studies

An improved gold pattern was designed specifically for long-term implantation studies. The new pattern needed to be smaller than Hollenberg's design, as the rat would be supporting the weight of the electrode while awake and moving during chronic implantation. In addition, the new design needed to be capable of a simple, lightweight connection with a data recording system or transmitter. The new pattern was designed in this case for 2 0.4mm 32 pin board-to-board connectors from Japan Aviation Electronics Industry Ltd. (Tokyo, Japan). The pattern is shown in Figure 3.7.

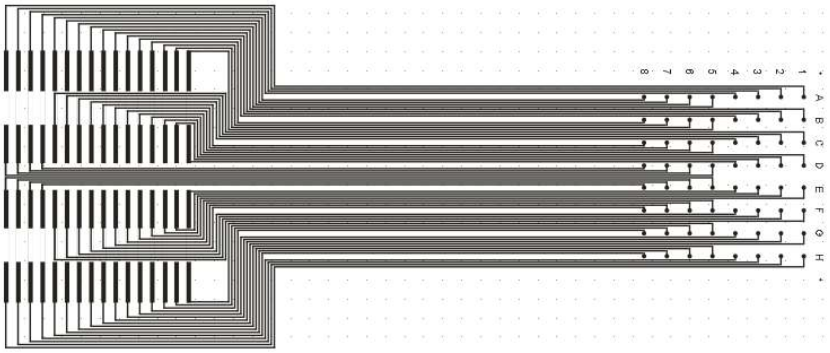

Figure 3.7 Streamlined pattern for chronic implantation

The 8x8 grid array is the same as before, but the connecting traces are now 50μm for the entire length of the pattern. The spacing between pads is 400 μm, which aligns with the 32 pin connector. The SU-8 pattern also was updated, not only to reflect the changes in the gold design but also to expose a slightly smaller area over the connector pads than the gold design. This allowed for some constraint of the gold by the SU-8 to help avoid delamination from connecting stress buildup. The protective SU-8 is shown in Figure 3.8.

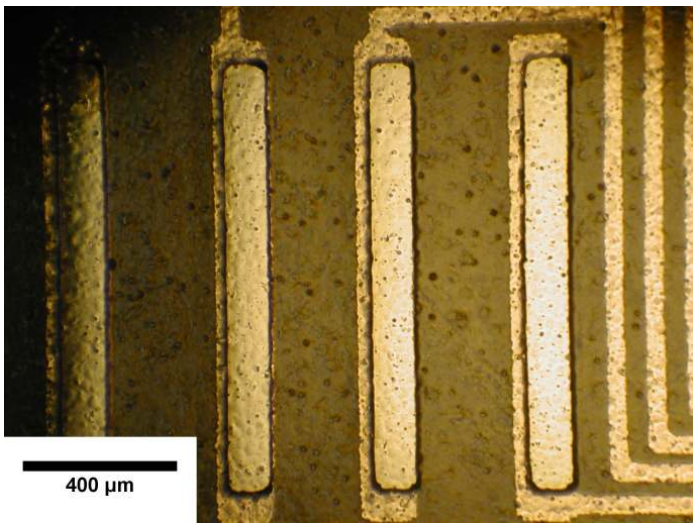

Figure 3.8 SU-8 coating over the gold pattern, showing partial coverage of connector pads for protection

The SU-8 exposed area size corresponds to the actual size of the connecting pins in the JAE board-to-board connector. Silver epoxy or a conductive film could be used to attach the connector to the electrode, but precise alignment under a microscope is necessary for this design.

Chapter 3.4 Electrical Testing Prior to Implantation

After the electrode arrays had individually been stamped, it was necessary to test the impedance values of each electrode channel. Impedance was chosen as the critical quantity to measure due to the high frequency (~1kHz) of the neural firings in the rat.[4] The impedance of each channel was measured using an Agilent 4294A precision impedance analyzer. A small amount of Ringer's solution was placed over the 8x8 grid of gold pads and a probe tip was placed in the saline while the other probe tip measured

each channel at the end of the connection setup. A typical 64 channel impedance chart is shown in Table 3.1.

Table 3.1 Typical impedance values for an array (kΩ). Italics indicate an open circuit.

47	34	34	30	43	29	38	18
43	31	28	24	28	28	26	*9000*
27	14	25	23	24	28	*8000*	27
26	14	26	16	25	24	47	32
23	13	27	*12000*	24	28	27	23
28	12	*10000*	28	32	180	21	25
25	32	27	29	28	148	19	24
28	37	33	47	31	40	29	32

As can be seen in the table, usually around 60 of the 64 channels survive the microfabrication procedure with a good impedance. It should be noted that the array has exceptionally good signals compared to the impedances of some microelectronic arrays. Takeuchi et al reported an array with average impedance of ~1 MΩ[4], while Prigg et al had impedances of 3-5 MΩ during their rat recordings[5]. Thus, working channels in the kΩ range is a significant improvement over these arrays.

Chapter 3.5 Implantation of Characterized Electrode Arrays

Once the electrical connectivity was verified with the impedance analysis, long term cortical signal recording could begin. For initial chronic testing, 6 to 12 channels were cut from working electrodes and implanted. The small electrodes were chosen to test the viability of the chronic implantation, with the ultimate goal of implanting a full 64 channel array after the process had been verified. These electrodes were also made with the old standard of including a TiW adhesion layer with the gold. Subsequent testing

determined that better adhesion layers could be included, but the initial studies all were Au-TiW-Kapton. Full, optimized electrodes should follow the same procedure in this section.

Electrode arrays were implanted on the surface of the cortex in female Sprague-Dawley rats, shown schematically in Figure 3.9. All surgical procedures were performed in accordance with the "Guide for the Care and Use of Laboratory Animals" approved by the Washington State University Animal Care and Use Committee. Isoflurane (5.0%) was used to induce anesthesia followed by maintenance of anesthesia (1.0-2.0%) in oxygen. Toe pinch reflex, heart rate, and respiration were used to track the depth of anesthesia. A 5 x 1mm area of bone was removed 1mm medial to the temporal ridge and 1 mm rostral to lambda, and the gold on Kapton electrode array was inserted between the bone and the dura over the auditory and somatosensory cortex. A stainless steel screw electrode was placed over the frontal lobe to determine the behavioral state of the animal, and another over the parietal lobe next to the gold electrodes as a control electrode. Two screws placed over the occipital lobe served as a ground reference. One dose of penicillin (0.1 mL IM each leg, total dose = 10,000 iu/kg) was given at the end of the surgery.

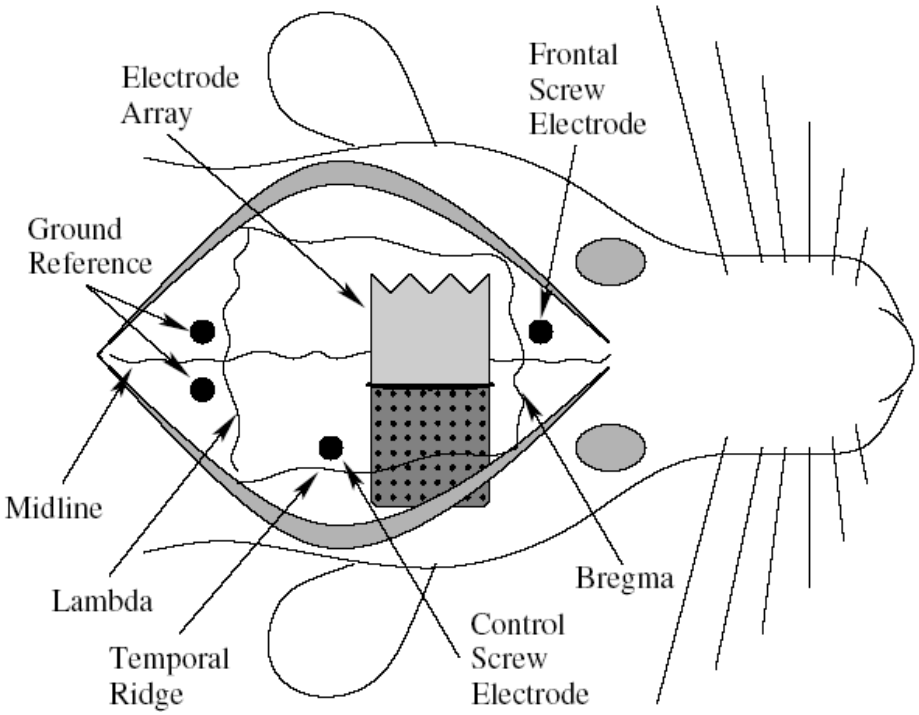

Figure 3.9 Placement of the electrode array in a Sprague-Dawley rat

Flunixin (1.1 mg/kg Sbc.) was given as a pain reliever and anti-inflammatory agent for 3 days after the surgery. Two weeks of surgical recovery elapsed before recording commenced.

One week after recovery from surgery, animals were connected to a customized amplifier system and tethered through a thin cable and commutator which allowed free movement with in a 30x30x50cm box. The auditory cortex was stimulated using speaker clicks (200μs pulse) at random intervals of 1-2s for 30 minutes. The electrical signals from the electrodes were filtered between 0.1 Hz and 3.2kHz, then sampled at 10 kHz using a custom data system[6]. The system recorded about 1,200 evoked response potentials (ERP) per session and the average ERP amplitude was calculated for each gold and screw electrode.

Chapter 3.6 Four Point Bend Test Specimen Preparation

For all four point bend tests, the specimens were prepared up to the point of patterning and etching. Thus the starting specimen was a film of metal on the polyimide. Silicon substrates were prepared by using a diamond-tipped scribe and a ruler to carve notches for rectangular specimens in 3 inch Si wafers. A slight amount of applied bending tension to the notch results in immediate, crisp fracture along the notch. This allowed for simple but precise Si substrates. A schematic of the silicon sample preparation is shown in Figure 3.10.

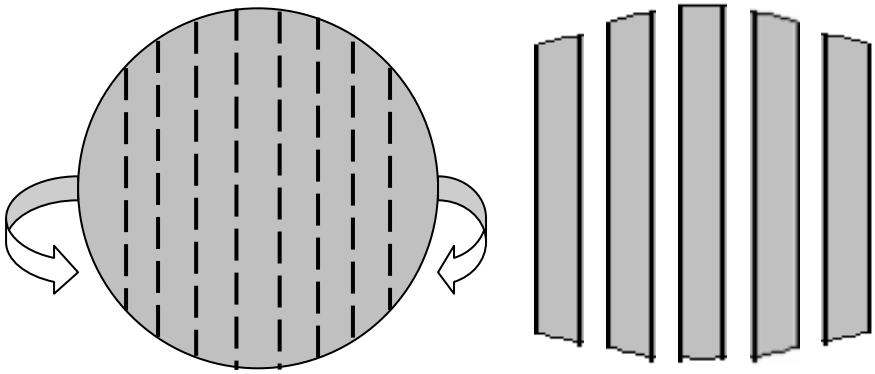

Figure 3.10 Rectangular samples notched and snapped from a Si wafer

The silicon rectangles were then brought into the clean room, where the rest of the four point sample preparation takes place. The silicon pieces were cleaned with the five step cleaning process in the clean room. Plain pieces of Kapton were then cut into samples of roughly the same size as the silicon samples and five step cleaned as well. The metal-Kapton samples were also cut into appropriately sized pieces and cleaned. These films were then scored with a razor on the middle of the Kapton side in the transverse direction to the piece length. This was to ensure that the crack passed through

the Kapton into the metal-Kapton interface rather than possibly delaminating the Kapton from the silicon. Then one sample of the plain Kapton and one sample of the metal-Kapton were then bonded to silicon substrates with Epon 440 epoxy (3M, St. Paul, MN) and also to each other, as illustrated in Figure 3.11. A couple drops of epoxy were placed on each silicon piece, and then the Kapton was pressed onto the piece, ensuring even spreading of the adhesive. The Kapton – Si samples were then heat cured at 150°C for 30 seconds. The two pieces were bonded together with two or three drops of epoxy and held securely during the cure stage with alligator clips. Typical cure times were seven to ten minutes to ensure all of the epoxy had completely hardened. The precise placement of the score in the metal-Kapton system was demarcated with a permanent marker for notching the silicon later.

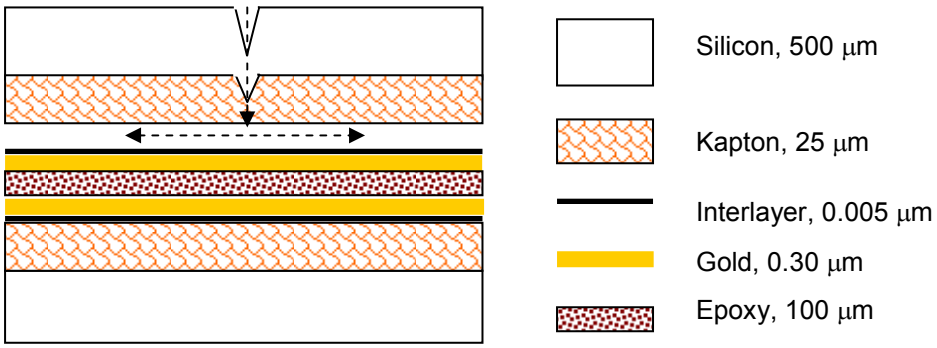

Figure 3.11 A cross section of the bend test sandwich specimen, showing the probable crack path

After the curing had been completed, one side of the four point specimen was notched with a diamond-tipped scribe. The notch was aligned with the score in the Kapton. The crack path shown in Figure 3.11 assumed that the crack preferentially

propagated through the polyimide rather than delaminating it from the silicon. Note that the figure is not to scale; the thin layers are enlarged in order to show detail.

The specimens were tested in a uniaxial compression loading system as shown in Figure 2.1. The system measured applied load and displacement using LabView software and a Honeywell Model 31 load cell with a maximum error of 2.5% (Spokane, WA). The loading rate was 1.0μm/s, applied with a Parker linear motor (Redmond, WA), and the loading continued until the crack had completely broken through the sample. Sample dimensions were measured with a micrometer to an accuracy of 0.01 mm. An average of at least three points was taken for each dimension measurement. A detailed error analysis is presented in the appendix. After the test, the sample pieces were specially labeled and kept for optical microscopy and / or chemical analysis to ascertain which interface contained the crack propagation and which layer delaminated.

References

[1] B.A. Hollenberg. A MEMS Based Electrode Array For Cortical Surface Potential Recordings. Masters Thesis, Washington State University, December 2005.

[2] T.A. Jan, L. Lu, C. Li, R.W. Williams, and R.S. Water. Genetic analysis of posterior medial barrel subfield (PMBSF) size in somatosensory cortex (SI) in recombinant inbred strains of mice. BMC Neuroscience 9, 3 (2008) 1-13.

[3] L. Supriya and R.O Claus. Solution-Based Assembly of Conductive Gold Film on Flexible Polymer Substrates. Langmuir 20 (2004) 8870-6.

[4] S. Takeuchi, T. Suzuki, K. Mabuchi, and H. Fujita. 3D flexible multichannel neural probe array. Journal of Micromechanics and Microengineering 14 (2004) 104–7

[5] T.Prigg, D. Goldreich, G.E. Carvell, and D.J. Simons. Texture discrimination and unit recordings in the rat whisker/barrel system. Physiology and Behavior 77 (2002) 671-5.

[6] D.M Rector and J.S. George. Continuous image and electrophysiological recording with real time processing and control. Methods 25, 2 (2001) 151-63

CHAPTER 4

EFFECT OF PLASMA ETCHING ON METAL ADHESION

This chapter presents research into surface chemistry treatment of the polymer film in order to increase adhesion of the conductive metal film. Surface treatment was chosen as an adhesion-promoting mechanism so that increased device reliability could be achieved without major changes in mechanical properties of the finished electrode array. Four point bend tests were used to measure the adhesion of the film – substrate system and quantitatively determine the effectiveness of pre-treatment of the Kapton prior to sputter deposition of the gold film. The only major treatment studied was oxygen plasma etching under a vacuum.

Chapter 4.1 Oxygen Plasma Etching of Polyimide Surfaces

Plasma etching with oxygen has been found to increase adhesion between metals and polyimides through opening of the imide rings and creating extra C-O and C-OH functional groups.[1] Figure 4.1 shows an normal monomer of the polyimide Kapton.

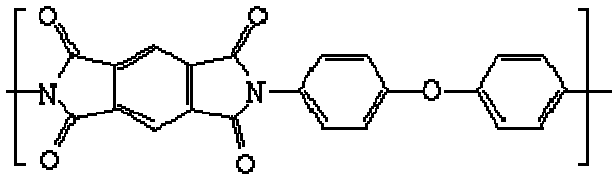

Figure 4.1 Chemical structure of Kapton

The formation of C-O and C-OH groups can be observed via x-ray photoelectron spectroscopy (XPS) as in Figure 4.2. The evolution of the new functional groups is seen in Peak 3 of Figure 4.2(b). One result of the new groups is an increase in hydrophilic

character of the polyimide surface.[2] This has been quantified elsewhere for Kapton specifically using dynamic contact angle measurements, showing that an increase in etching power leads to a decrease in the contact angle of water (i.e. better wetting).[3] Similar functional group alterations are observed for DC and RF oxygen plasma etching.[1]

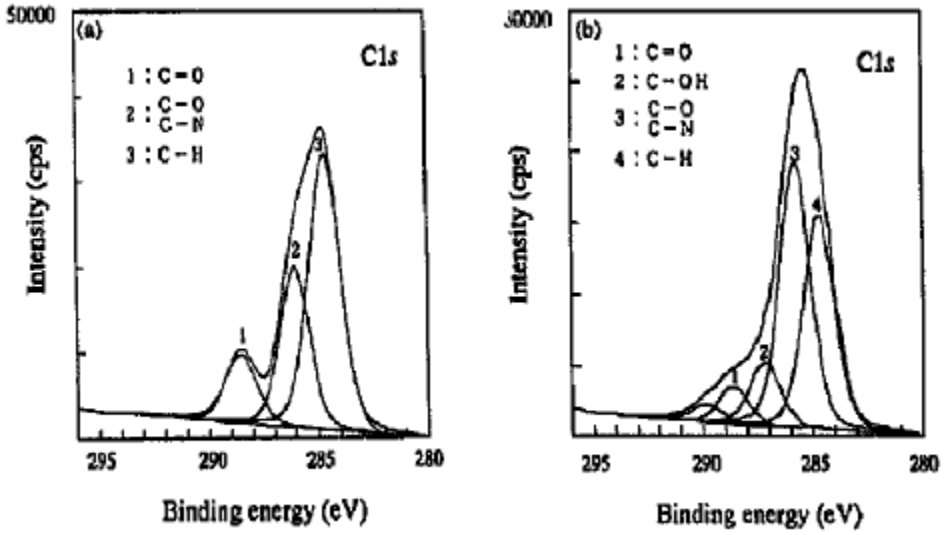

Figure 4.2 Carbon 1s XPS Spectra for a) untreated polyimide and b) microwave oxygen plasma etched polyimide[2]

In some cases, the increase in adhesion is such that a peel-induced fracture occurs not at the interface but inside the polyimide at the depth of the ion bombardment.[4] Oxygen plasma etching has been shown specifically to increase adhesion of gold to Kapton, though not quantified in more detail than tape peel strength or amount of delamination in a pull-off test.[5]

An added effect of the etching is a tendency to roughen the surface, which may increase physical interlocking of the deposited metal with the surface, but certainly increases ionized surface area. Interlocking is the mechanical increase in bond strength due only to physisorption, while increases in strength due to increased surface area are

dependent on the type and number of chemical bonds formed. Copper and chromium have shown increased adhesion to Kapton surfaces roughened with oxygen plasma etching. The adhesion, measured by T-peel testing, improved by as much as 220% as the surface roughness increased. The authors of the study admitted, however, that it was impossible to differentiate between improvement due to increased surface area and improvement due to interlocking.[6] A detailed study using scanning force microscopy has determined that polyimide surface roughening has little to no effect on physical interlocking, instead only finding evidence of increased functional group bonding. This was verified by creating identical polyimide surface morphologies with both oxygen and argon plasmas and measuring non-identical metal adhesion values. In addition, the study found that metal adhesion increased with etching time even though the surface roughness did not. Since surface ionization and creation of functional groups increased with etching time and with changes in plasma chemistry, the increase in adhesion could only be attributed to surface chemistry changes and not to mechanical interlocking.[7]

Another method often used to increase adhesion in polymer-metal systems is deposition of a primer layer. Comparison of adhesion improvement for several different primer layers would give insight into the mechanisms of the adhesion increase in gold-Kapton systems due to the plasma etching. Specifically, if each adhesion-promoting layer showed uniformly increased interfacial toughness after plasma etching, it would indicate that surface chemistry may not be as important as surface roughness or other physical factors altered by ion bombardment. On the other hand, if one particular metal layer showed marked improvement, it may signify that the interfacial interactions of the metal and the polyimide are strongly dependent on surface chemistry.

Two metal primer layers were chosen to investigate this process. An alloy of titanium and tungsten (90%W by weight) has been found to improve gold adhesion in some microelectronic systems, so a thin layer of TiW between the gold and Kapton was utilized as a pre-treatment.[8,9] Tantalum has also been used classically to improve gold adhesion to various substrates, so it was chosen as another metal adhesion layer.[10] Both layers were compared to gold-Kapton adhesion with and without the plasma treatment, yielding a total of six interfacial toughness data sets.

Chapter 4.2 Specimen Preparation

The plasma etching, metal deposition, and four point bend test sample preparations were all performed in a Class 1000 clean room, as described in Chapter 3.6. On a cleaned Kapton surface, each of the previously described possible pretreatments to improve the adhesion of gold to the Kapton were performed. A set of samples was fabricated for each of the following conditions: a three minute O_2 plasma etch of the Kapton surface, 5 nm of TiW or Ta sputtered before the gold, both treatments, and neither treatment. The processing pressure for the oxygen plasma was 135 mtorr and the RF voltage was 100 W. After a pretreatment, 300 nm of gold was DC Magnetron sputtered onto the treated surface as described in Chapter 3.1. No patterning was carried out, as blanket films are easily assessed using the four point bend test.

Once all the metal deposition had been performed, the samples were subjected to another 3:00 O_2 plasma etch to remove organic contaminants. The non-coated surface of each sample was then attached to a cleaned elastic substrate using cyanoacrylate glue or an epoxy. The samples were bonded to the substrates, either Si or SiO_2, in an effort to

gain rigidity and therefore the ability to undergo four point bending. Two samples would then be sandwiched together using epoxy[11,12,13] and cured at 150°C. One side of the sandwiched specimen was then notched by a diamond-tipped blade to initiate a crack site, as shown in Figure 4.3, reproduced from Figure 3.9. For a more detailed sample preparation procedure, refer to Chapter 3.

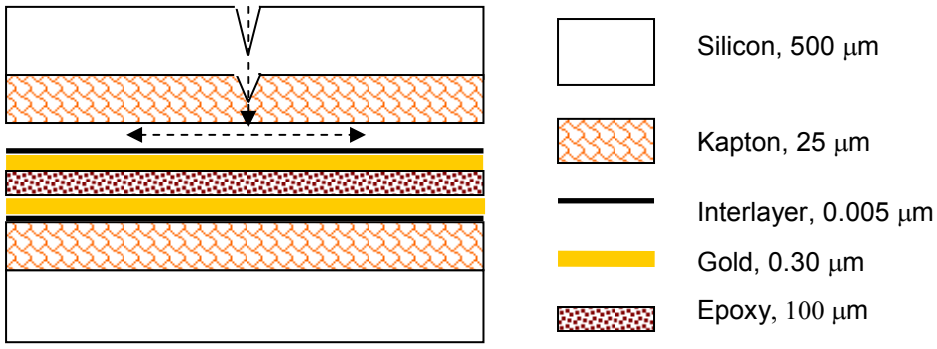

Figure 4.3 The typical sandwich specimen

Chapter 4.3 Four Point Test Results and Discussion

Samples were placed into the testing apparatus so that the pre-crack would be in tension under the applied load, in accordance with the four point bend test theory presented in Chapter 2. The bend test operated under constant displacement in only one direction. Figure 4.4 shows a typical constant displacement loading curve, with regions of interest demarcated on the graph. As can be seen in Figure 4, the notched slide typically fractured around 20N, which was well within the range of the load cell. Four point bend tests were performed on several specimens for each pre-treatment condition. After the crack had propagated through the entire specimen, optical examination was made to determine which interface had fractured.

The plateau in the load – displacement curve that follows the initial breakthrough is used to calculate crack growth resistance of the interface. In comparison with loading curves for thin films on elastic substrates, the curves generated from this project do not generally have a crisp, obvious plateau.[11] The effect of loading rate on the load plateau has been discussed elsewhere and may provide some insight here. The rate used for these specimens is approximately twenty times faster than an advised loading rate for accurate results.[13] However, the elastic-plastic nature of this system forces consideration of plastic deformation effects, specifically creep. The faster rate was chosen in an effort to avoid time-dependent, rather than load-dependent, deformation. This necessity may account for the relative non-linearity of the plateau.

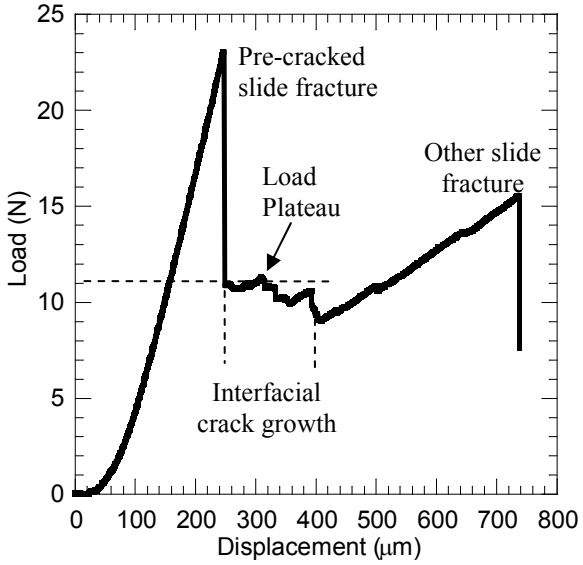

Figure 4.4 Typical load vs. displacement curve for plasma etched samples with a TiW adhesion promoting layer

For providing a comparative assessment of adhesion values, a horizontal linear curve fit was applied to the region directly following the first breakthrough, as seen in Figure 4.4. Using Equation 1 from Chapter 2 with the measured plateau loads, the energy

release rate of the various treatments are shown in Table 4.1. It should be noted that some of the experimental parameters are different for the various adhesion layers – this was done in an effort to reduce the amount of scatter amongst data points with some positive effect.

Table 4.1 Interfacial adhesion energy values for various pre-treatments (J/m^2).

	Plasma Etch	No Plasma Etch	Improvement	p value[(c)]
No TiW Layer[(a)]	2.5 ± 0.8	1.9 ± 0.8	31%	0.66
TiW Layer[(a)]	2.6 ± 0.8	1.7 ± 0.8	53%	0.1
Ta Layer[(b)]	2.3 ± 0.5	1.4 ± 0.5	64%	0.2

(a) Constant displacement rate of 10μm/s, SiO_2 substrate (b) Rate of 1μm/s, silicon substrate

(c) Wilcoxon–Mann–Whitney rank sum unpaired test for independence

Table 1 summarizes the four point bend test results. Three or four specimens for each pre-treatment condition were used to determine these values, making a standard deviation inappropriate for comparison – the deviation reported in the table is the total range of experimental values. The p value reported here is the independence of each plasma etched data series from the non-etched series. Details regarding the Wilcoxon-Mann-Whitney test can be found in the appendix. A value of 0.05 demonstrates complete independence, and while the data presented here do not qualify, there is at least a noticeable difference for the TiW and Ta samples.

After fracture, each specimen was examined to determine along which interface the crack had propagated. Energy release rates were only calculated from the load – displacement data if either of two conditions were met: first, if there was clear visual evidence of delamination of the gold from the Kapton; second, if the failing interface was

the cyanoacrylate – Kapton interface. The second condition was included in the measurements because the glue always failed at higher loads than any of gold – Kapton delaminations (the toughness of the cyanoacrylate – Kapton interface was 3.2 J/m^2). While this inherently adds some uncertainty to the specific values of the interfacial energies reported in Table 4.1, the inclusion allows for a larger sample set and therefore more statistically valid trend analysis. The methodology to compute these values can therefore be described as a conservative estimate, since the interfaces sometimes were stronger than the test allowed for measuring. However, it is possible that plasticity of the Kapton acted as a barrier to crack propagation, forcing cyanoacrylate delamination rather than allowing the crack to reach the gold-Kapton interface. Therefore the values listed in Table 4.1 should be considered as an isolated study, not directly comparable with other adhesion values in this thesis.

The principal result from the four point bend tests is the qualitative confirmation that a surface treatment of the Kapton with plasma significantly increases its adhesion to gold. While the values listed in Table 4.1 are specifically accurate only in the purely elastic case assumed in the crack propagation energy equations, the relative interfacial strengths are first order extension to this particular elastic-plastic system. It should also be noted that direct comparison of Ta and TiW adhesion layers cannot be made using Table 4.1, due to the reasons mentioned above as well as varying loading rates, and in fact a valid comparison is made in Chapter 5 by restricting the data so that only identical experimental parameters are used.

Some insight into the specific strengthening mechanisms of the plasma etching can be gained by investigating the non-uniform adhesion improvements for the various

metal layers. As seen in Table 4.1, Ta demonstrated the most noticeable plasma etching effect, followed by TiW and then Au. This disparate increase is seen despite identical processing parameters, indicating that the effect is purely chemical. Pearson used the Fowkes-Drago approach to characterize adhesion of polyimides at the molecular level.[14] Equation 1 was used to quantitatively determine the strength of the primary and secondary bonds,

$$-\Delta H^{AB} = E_A E_B + C_A C_B \qquad (1)$$

where the ΔH is the heat of mixing of components A and B, E is an electrostatic contribution constant to the bond strength, and C is a covalent contribution constant. E and C are known as Drago constants, and can be measured from flow microcalorimetry or contact angle measurements. Pearson found Drago constant values for two epoxies and successfully used them to predict relative adhesion strength of the epoxies to a polyimide. However, a literature search has not produced Drago constants for the metals used in this study, nor indeed any verification that the Fowkes-Drago equation can be applied to metal-polymer, rather than polymer-polymer, interfacial interactions. Flow microcalorimetry, infrared spectroscopy, x-ray photoelectric spectroscopy, and dynamic contact angle measurement techniques potentially could be employed to determine values of the Drago constants for the gold-Kapton system, but that is beyond the scope of this research.

Chapter 4.4 Summary and Conclusions

Four point bend testing has been used to quantify the adhesion promoting effect of oxygen plasma etching prior to sputter deposition. The metal-polymer interfacial

energy values are useful as a first-order approximation, due to possible plastic effects such as creep, but still give meaningful experimental data to reinforce that plasma etching appears to increase the toughness of the Au – Kapton system by approximately 30%. Even greater increases in toughness are observed for TiW and Ta layers, leading to the insight that evolved functional group – metal bonding is primarily responsible for the increased adhesion, rather than amount of exposed surface area or Kapton etched morphology. It is anticipated that an ideal adhesion layer could be identified from bond strength calculation using Equation 1, assuming that Drago constants could be measured and applied for a metal-polymer system. Additionally, literature reports of metal adhesion to hydroxyl and carboxyl groups may be useful for predictive purposes.

References

[1] F.D. Egitto and L.J. Matienzo. Plasma modification of polymer surfaces for adhesion improvement. IBM Journal of Research & Development 38, 4 (1994) 423-39.

[2] Y. Nakamura, Y. Suzuki, and Y. Watanabe, Effect of oxygen plasma etching on adhesion between polyimide films and metal, Thin Solid Films 290 (1996) 367-9

[3] M. Lindeberg and K. Hjort. Interconnected nanowire clusters in polyimide for flexible circuits and magnetic sensing applications. Sensors and Actuators A 105 (2003) 150-161

[4] D.L. Pappas, J.J. Cuomo. Studies of adhesion of metal films to polyimides. Journal of Vacuum Science & Technology A 9, 5 (1991) 2704 – 08

[5] L. Supriya and R.O. Claus. Solution-Based Assembly of Conductive Gold Film on Flexible Polymer Substrates. Langmuir 20 (2004) 8870-6

[6] S.H. Kim, S. W. Na, N.E. Lee, Y. W. Nam, and Y. Kim. Effect of surface roughness on the adhesion properties of Cu/Cr films on polyimide substrate treated by inductively coupled oxygen plasma. Surface & Coatings Technology 200 (2005) 2072 – 2079.

[7] C.D. Dimitrakopoulos and S.P. Kowalczyk. Scanning force microscopy of polyimide surfaces. Thin Solid Films 295 (1997) 162 – 8

[8] P. Jalonen and A. Tuominen, The effect of sputtered interface metallic layers on reinforced core laminate making build-up structures. Microelectronics Reliability 42 (2002) 1075–9

[9] R.J. Gutmann , T. P. Chow, S. Lakshminarayanan, D.T. Price, J.M. Steigerwald, L. You, and S.P. Murarka. Integration of copper multilevel interconnects interlevel dielectrics with oxide and polymer. Thin Solid Films 270 (1995) 472 – 9

[10] K.E. Haq, K.H, Behrndt, and I. Kobin. Adhesion Mechanism of Gold-Underlayer Film Combinations to Oxide Substrates. Journal of Vacuum Science & Technology A 6 (1969) 148–52

[11] R.H. Dauskardt, M. Lane, Q. Ma, and N. Krishna. Adhesion and debonding of multi-layer thin film structures. Engineering Fracture Mechanics 61 (1998) 141-62

[12] Z. Huang, Z. Suo, G. Xu, J. He, J.H. Prévost, and N. Sukumar, Initiation and arrest of an interfacial crack in a four-point bend test. Engineering Fracture Mechanics 72 (2005) 2584-601

[13] M.P. Hughey, D.J. Morris, R.F. Cook, S.P. Bozeman, B.L. Kelly, S.L.N. Chakravarty, D.P. Harkens, and L.C. Stearns. Four-point bend adhesion measurements of copper and permalloy systems. Engineering Fracture Mechanics 71 (2004) 245-61

[14] R.A. Pearson. Adhesion Studies for Flip-Chip Assemblies. Adhesive Joining and Coating Technology in Electronics Manufacturing (2000) 35 - 40

CHAPTER 5

FOUR POINT BEND TESTING OF VARIOUS ADHESION LAYERS

This chapter summarizes the results of four point bend testing of the gold-Kapton system with an assortment of adhesion promoting layers. The four point bend testing of sandwich specimens proved suitable for identifying the effectiveness of different layers in a quantitative fashion. Tantalum, titanium, and a titanium-tungsten alloy were primarily chosen for testing due to their biocompatible nature, though tantalum requires further testing before it is allowed for use in brain implantation. Chromium was selected in order to provide a non-implantable standard by which the other adhesion layers could be compared. Other adhesion promoting layers can be tested with this method in order to make the most reliable electrode possible.

Chapter 5.1 Adhesion Promoting Layer Selection

Four different adhesion layers were four point bend tested: a titanium-tungsten alloy (10%Ti-90%W by weight), pure titanium (Ti), pure tantalum (Ta), and pure chromium (Cr). Under certain conditions, chromium may be a suitable adhesion layer for implantable electrodes,[1,2] and some chromium alloys may be non-toxic for neural implantation,[3] but these results require further testing. Tantalum has also been used classically to improve gold adhesion to various substrates, but it also yields somewhat poorer results than chromium.[4] Additionally, tantalum may be biocompatible for prosthetics but is considered "reactive" for neural implantation.[3,5] Both titanium and

tungsten are considered biocompatible and non-reactive and have been used in neural interfaces as an adhesion layer for gold.[6,7]

Chapter 5.2 Sandwich Specimen Testing

All samples were fabricated as described in Chapter 3.5, with the exception of the exact arrangement of the film stack. Initial four point bend tests showed that sandwiching two gold-Kapton layers was fruitless as only one interface ever delaminated. In an effort to maintain symmetry, an untreated Kapton layer was used as the second half of the specimen. Thus, the only layers missing were the 300 nm of gold and the 5-10 nm of adhesion layer, which are not expected to significantly alter the geometry of the specimen. The modified film stack is illustrated in Figure 5.1.

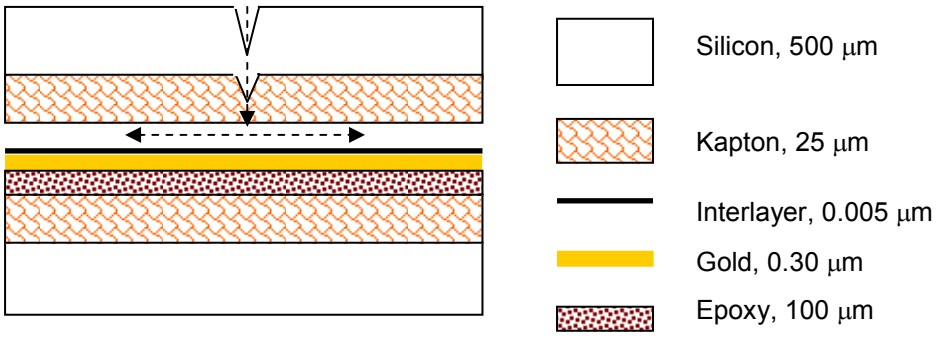

Figure 5.1 Modified film stack used for adhesion layer testing, with crack path

Before metal deposition, all samples were pre-treated with a 3:00 oxygen plasma etch, as described in Chapter 3.1. Each four point specimen in the adhesion layer study used silicon wafers as the elastic substrate, with epoxy bonding the Kapton to the silicon and the samples to each other. After fabrication, the specimens were tested in a uniaxial loading system in the manner indicated by Figure 2.1 in Chapter 2. LabView software

recorded load and real-time displacement data during the test. Every specimen tested for this study was loaded at 1.0 μm/s. Samples were monitored throughout the test to verify that the crack path indeed propagated laterally, causing delamination of some interface, at a point prior to total specimen fracture. Due to the complex nature of the four point bend test sandwich specimens, it was necessary to ensure that the interfacial energy that was being calculated was for the correct interface. Several interfacial crack paths were possible: between the metal and the polyimide, between the polyimide and the silicon, or between the metal and the epoxy. Precise identification of the delaminating interface was not possible during the test, so a combination of optical microscopy and X-ray photoelectron spectroscopy (XPS) was used to determine the delaminating interface after testing.

Chapter 5.3 Bend Test Results

Figure 5.2 shows typical load-displacement curves from the four point bend tests using each of the interlayer materials.

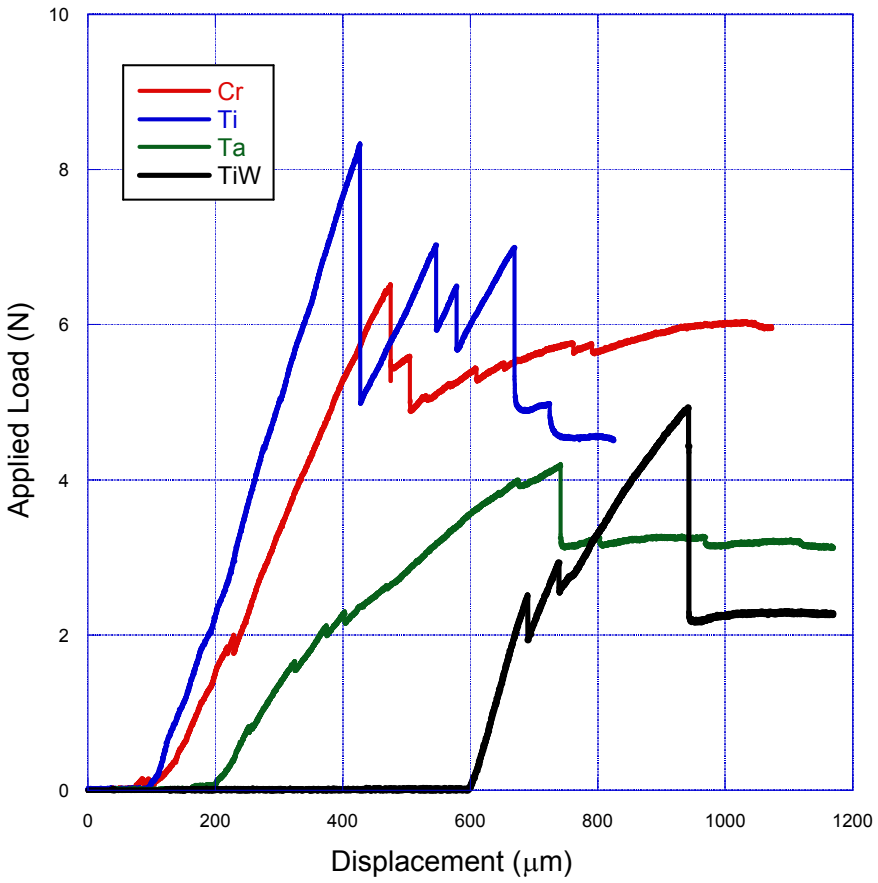

Figure 5.2 Typical load – displacement curves for all four adhesion layers

As previously seen in Figure 4.4, each specimen which exhibited interfacial delamination has a load plateau in the load-displacement curve. It should be noted that the load plateau value is the important parameter in Figure 5.2, not the maximum load before the initial breakthrough. The maximum load is not a function of layer strength – rather, it is determined by the size and stiffness of the elastic constraining substrate. Not all samples were exactly the same size, and this is accounted for in the actual crack extension energy calculations.

Optical inspection of a typical fracture surface reveals that there is exposed Kapton without the gold coating, indicating that gold-polyimide delamination was

occurring during the test. Figure 5.3 is a schematic explaining terminology to be used later in this chapter, and will assist in comprehending the optical micrographs in Figures 5.4.

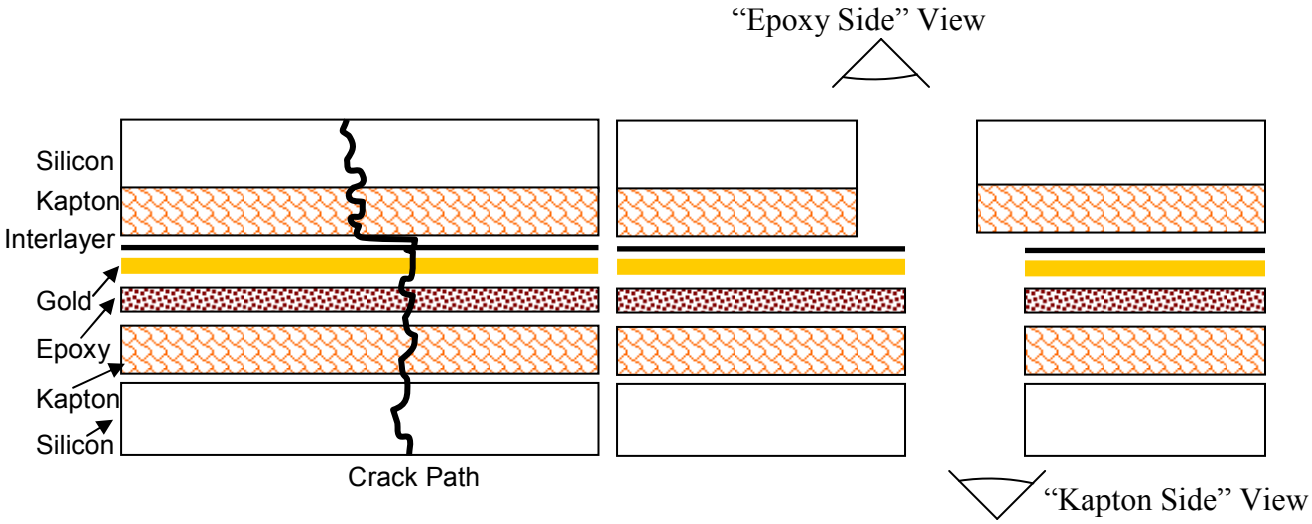

Figure 5.3 Terminology definition for typical fracture path observation

When viewing the fracture surface under an optical microscope, it was possible to see one of two things for a given view. If the "epoxy side" view revealed gold at the fracture surface, as shown in Figure 5.3, then the gold delaminated from the Kapton and the test was a success. However, if the "epoxy side" view only revealed the epoxy, then the delaminating interface was the gold-epoxy interface. The opposite is true for the "Kapton side" view; observation of gold at the fracture in this case meant gold-epoxy delamination, while observation of epoxy or uncoated Kapton meant gold delamination. Figure 5.4 (a) and (b) are optical micrographs of successful gold-Kapton delamination. Figure 5.4 (a) is from the Kapton side view, while (b) is from the epoxy side view.

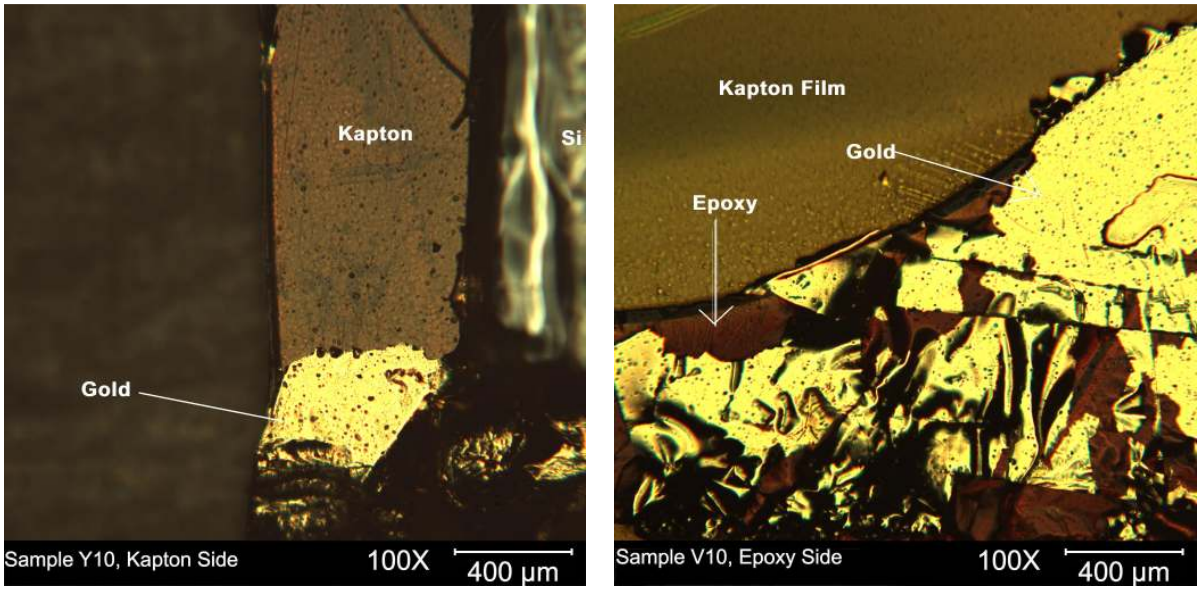

(a) (b)

Figure 5.4 Kapton side view (a) and epoxy side view (b) of four point bend fracture surface

In both micrographs, there are clearly regions of delamination. However, the delamination is not uniform, which may be part of the reason for the non-linearity of the load plateaus in Figure 5.2, in addition to the reasons listed in Chapter 4. Nevertheless, delamination of the gold from the Kapton definitely occurs in the four point bend test sandwich specimens.

While visual inspection suggests metal-polyimide delamination, it was not possible, using optical microscopy, to definitively state whether the delamination was between the adhesion layer and the Kapton or between the adhesion layer and the gold. Therefore XPS, using a AXIS-165 model (Kratos Analytical, Inc., Chestnut Ridge, NY), was performed on the fracture surface, and the resulting spectra for a sample with a Ti-W adhesion layer is shown in Figure 5.5. The binding energy was calibrated against gold (Au) 4f 7/2 to be 84 eV and highly ordered pyrolytic graphite (HOPG) carbon (C), 1s at 284.5 eV. Peaks in the spectra are identified in Figure 5.5.

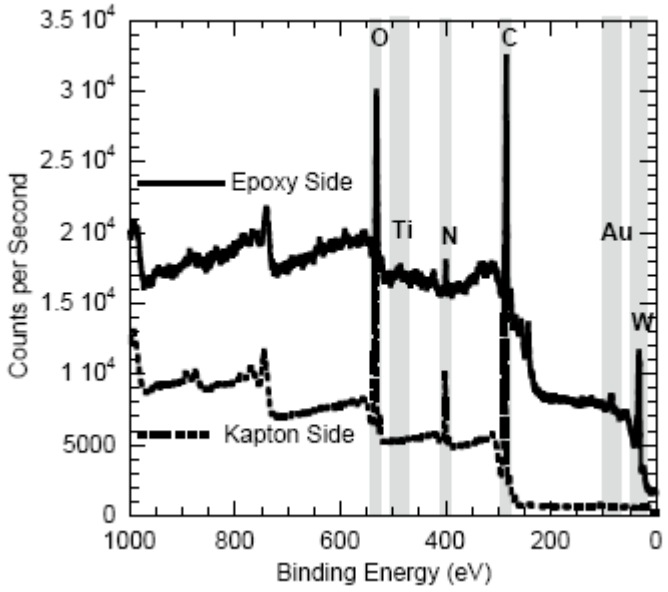

Figure 5.5 XPS spectra for the two sides of the fracture surface for Au-TiW-Kapton

Small peaks of Ti and Au and a large tungsten (W) peak on the "epoxy side" indicate that the TiW layer peeled away from the Kapton, unambiguously showing that the fracture occurred at the TiW-Kapton interface. This was a positive result, showing that the limiting factor to electrode reliability is indeed the delamination resistance of the adhesion layer rather than the gold (i.e. the gold was well adhered to the adhesion layer). The large nitrogen peak on the Kapton side was due to the nitrogen in the chemistry of the polyimide.

Chapter 5.4 Calculation of Fracture Toughness from Bend Test Results

Using the load plateaus from the load-displacement curves (as illustrated in Fig. 5.2) and recording the specimen geometric dimensions, Equation 1 from Chapter 2 was

used to calculate the interfacial adhesion energy for each system. The results are given in Figure 5.6 and Table 5.1.

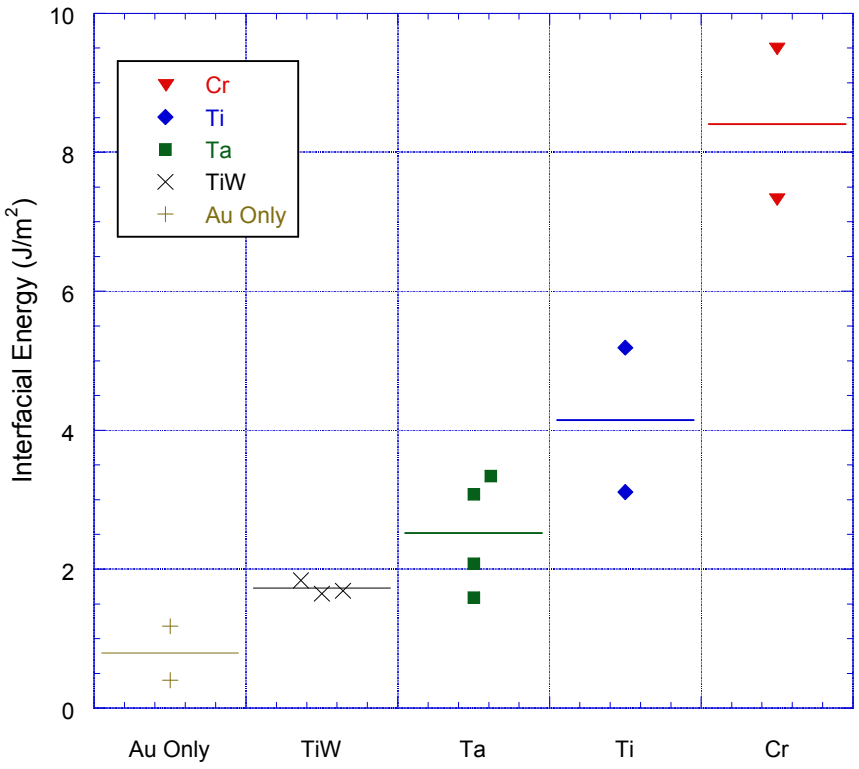

Figure 5.6 Interfacial toughness values for the tested specimens, compared to the specimens without adhesion layers (Au-only)

The bend test measurements indicate that Cr provides the best adhesion layer for the flexible electrodes of all of the systems tested in this study. However, for neural implantation the biocompatibility or toxicity of the metals must also be considered. TiW and Ti were chosen as a suitable adhesion layers for use in the long term implantation for their combination of durability and biocompatibility.

Table 5.1 Interfacial adhesion energy values for metal interlayers.

	Energy (J/m^2)	Standard Deviation	$p^{(a)}$
Au only	0.8	0.6	-
TiW	1.7	0.1	0.3
Ta	2.5	0.8	0.15
Ti	4.2	1.5	0.25
Cr	8.4	1.5	0.15

(a) Independence calculated from previous layer (e.g. Cr vs. Ti)

Table 5.1 summarizes the bend test results and gives the Welch-Satterthwaite t-test method p-value. The p-value is a measure of the independence of the two samples in question, and here is given as the comparison of each layer to its predecessor. Thus it is seen that samples utilizing a TiW interlayer outperform the gold-only samples with a 70% confidence, but Ta samples are tougher than TiW samples with an 85% confidence. Other comparisons of note not included in the table: Ti outperforms TiW with 75% confidence, and Ti is better than gold-only with 85% confidence. While Au-Cr-Kapton was the only 95% confident adhesion promoting layer with respect to gold-only, the relatively high confidence of the other layers was satisfactory for this study.

Chapter 5.5 Summary and Conclusions

Optical microscopy and XPS analysis verified that the four point bend test was useful for delaminating the gold and the adhesion layer from the Kapton. The horizontal load plateaus observed in the load – displacement plots were used to calculate crack extension energies, which are a measure of interfacial toughness. While the energies shown in the Figure 5.6 are quantitatively accurate only in the purely elastic case, the

relative interfacial strengths are a first order extension for this particular metal-polymer system. Thus, the four point bend test may be used for these polymer-metal systems to determine the relative increase in toughness provided by each adhesion layer. Chromium outperformed titanium, which outperformed tantalum, which outperformed the titanium-tungsten alloy, which was approximately twice as strong an interface as gold deposited upon plasma etched Kapton. Accounting for biocompatibility, it is the recommendation of this study that titanium, or at least titanium-tungsten, be used for all future electrode production.

References

[1] S. Mailley, M. Hyland, P. Mailley, J.A. McLaughlin, and E.T. McAdams. Thin film platinum cuff electrodes for neurostimulation: in vitro approach of safe neurostimulation parameters. Bioelectrochemistry 63 (2004) 359-64

[2] D. Soden, A. Morrissey, C. Collins, J. Piggott, J. Larkin, A. Norman, S. Aarons, C. Dunne, and G.C. O'Sullivan. Electrotherapy of tumour cells using flexible electrode arrays. Sensors and Actuators B 103 (2004) 219–24

[3] D.R. Merrill, M. Bikson, and J.G.R. Jefferys. Electrical stimulation of excitable tissue: design of efficacious and safe protocols. Journal of Neuroscience Methods 141 (2005) 171–98

[4] K.E. Haq, K.H. Behrndt, and I. Kobin. Adhesion Mechanism of Gold-Underlayer Film Combinations to Oxide Substrates. Journal of Vacuum Science & Technology A 6 (1969) 148–52.

[5] H. Matsuno, A. Yokoyama, F. Watari, M. Uo, and T. Kawasaki. Biocompatability and osteogenesis of refractory metal implants, titanium, hafnium, niobium, tantalum and rhenium. Biomaterials 22 (2001) 1253-62.

[6] S. Kim, K. Zoschke, M. Klein, D. Black, K. Buschick, M. Toepper, P. Tathireddy, R. Harrison, H. Oppermann, and F. Solzbacher. Switchable polymer-based thin film coils as a power module for wireless neural interfaces. Sensors and Actuators A 136, 1 (2007) 467-74

[7] P. Jalonen and A. Tuominen. The effect of sputtered interface metallic layers on reinforced core laminate making build-up structures. Microelectronics Reliability 42 (2002) 1075–9

CHAPTER 6

LONG TERM ACCELERATED IMPLANTATION TESTING

This chapter describes the methodology and results used to simulate long term implantation conditions in rats. Gold – Kapton samples were immersed in 60°C salt water and removed at 1, 2, and 10 weeks. The test was under accelerated conditions to gain some idea of chronic electrode performance prior to implantation so that no rats would be needlessly subjected to testing. Samples with and without adhesion layers were tested, but all samples had the standard 3:00 oxygen plasma etch described in Chapter 3 prior to sputter deposition of the metals.

Chapter 6.1 Accelerated Immersion Test Overview

Prior to actual electrode implantation in rats, an exploratory study in gold – Kapton behavior with a variety of adhesion layers under simulated implantation conditions was performed. The goal was to quantify changes in interfacial toughness as a function of exposure to ionic fluids in an effort to determine the long term reliability of the finished devices as well as to identify the mechanism by which the electrodes tended to fail. Observation of more than one failure mechanism would be of equal interest, even if it indicated the lifetime prediction was essentially impossible for this system.

Several possible mechanisms of failure for polymer – metal systems under long term implantation conditions were described in Chapter 1. In short, a literature review revealed two principal areas of concern: polymer swelling[1] and ion accumulation at the polymer – metal interface.[2] Some varieties of Kapton have been shown to swell as much as 2%, which was an obvious concern as studies in the gold – Kapton system specifically

had shown delamination and failure at only 1% strain.[3] Even if the Kapton used for supporting the electrode only absorbed a minimum of water and swelled to 0.5%, the strain caused by the swelling would increase the flow of ions to the interface. The ion accumulation could eventually cause blisters which would break the electrode channels. Due to the inert nature of both gold and Kapton, chemical reaction products with the saline solution were not anticipated, though if such a product did form with either the gold or the adhesion layer it could introduce defects at the interface, leading to failure. However, some of the adhesion layers could form oxides, leading to a volumetric change which would strain the interface and lower the fracture resistance.[4] This seems unlikely to have a large effect in the case of immersion in a solution, but it is a possibility.

Accelerated immersion testing was chosen as an investigative method because of several attractive qualities. The main advantage is that the test allowed for conservative estimates of long term electrode implantation. The lifetime prediction was conservative for the following reasons: first, the temperature was approximately 30°C higher than the body temperature of a rat, allowing for possible reactions to happen more quickly; second, the sodium concentration of the solution was approximately three times that of the fluid that would be in contact with the electrodes when implanted in the rat's brain; third, the immersion took place in liquid, while actual implantation would be in a diffusion-restricted mixture of solid and liquid; and fourth, no SU-8 protective coating was provided for this study. These factors all enhanced the likelihood of electrode failure by combining to increase the likelihood of diffusion into the interface, swelling of the polyimide, and any other mechanism that might lead to failure.

Chapter 6.2 Immersion Technique

Kapton samples were prepared for metal sputter deposition as described in Chapter 3.1 of this thesis. Some of those samples were given an adhesion layer, while some were not. Adhesion layers tested by the immersion process were titanium-tungsten (TiW) and chromium (Cr). 5 nm of TiW were deposited prior to the gold by DC sputtering for 0:51 at 100W and an argon pressure of 7.5×10^{-3} torr. 10 nm of Cr were deposited in 0:20 at 75W and an argon pressure of 7.5×10^{-3} torr. Then all samples were sputtered with 300 nm of gold using the standard recipe of 23:12 at 75W and an argon pressure of 7.5×10^{-3} torr. The specimens were not patterned or etched prior to immersion testing because the extra processing steps increased the chance of introducing defects. While there is a possibility for fabrication errors in all electrode manufacture, they do not typically affect all specimens in the same way. Thus all processing steps after deposition were avoided in order to maintain a consistent test across all samples.

Samples of metal – Kapton were immersed in a bath of saline solution consisting of 3% NaCl in de-ionized water. All of the samples were placed in the same saline solution to avoid deviation in saline content. The bath was then heated to 60°C, which it achieved in approximately one hour. Due to limited equipment availability, the bath was only heated from the bottom of the container, meaning that there was a slight temperature gradient, cooler near the top surface. However, all samples were loaded equivalently, so they all experienced the same testing conditions. De-ionized water was periodically added to the hot bath to counteract gradual evaporation of water in the solution.

Several Au and TiW-Au samples were removed after one and two weeks. This was because they had previously shown to be the weakest samples under four point bend

test inspection, so it was anticipated that they would show a relatively immediate drop in adhesion energy to the Kapton. After gentle rinsing with de-ionized water, four point bend test specimens were manufactured from the pulled samples as described in Chapter 3. After ten weeks, all remaining immersion test samples were removed from the saline solution. All viable samples were then four point bend tested.

Chapter 6.3 Four Point Bend Testing Of Immersion Samples

Attempts were made to fabricate four point bend test specimens from all of the immersion test samples. However, some of the samples degraded during the fabrication procedure. The rest of this section will detail the results by test length and adhesion layer.

Chapter 6.3.1 One and Two Week Specimens

Despite the accelerated nature of the durability test, the one and two week Au-Kapton and Au-TiW-Kapton specimens showed little sign of degradation. The only difference between the immersed samples and as-deposited samples was a slight optically observed dullness of the gold. None of the four point specimens delaminated gold from the Kapton – rather, the cyanoacrylate glue holding the Kapton to the glass slide was the failing interface, with a measured toughness of 3.2 J/m^2. At first glance, it may seem that this value can be taken as a conservative estimate of the actual fracture toughness of the gold-Kapton interface. Unfortunately, the fact that the crack propagated laterally along the first interface it reached only means that it was energetically favorable to delaminate the Kapton, rather than continuing vertically through the Kapton. This probably means that the notch in the Kapton, designed to allow propagation through the plastic layer, was

misaligned for these samples. However, it is also possible that some saline from the immersion test did not come off in the five step cleaning process, perhaps causing some poor adhesion between the cyanoacrylate and the Kapton. Since it was not desirable to employ a more rigorous cleaning process in consideration of accidental stress causing delamination of the gold, it was decided that all future four point bend tests would only use epoxy to attach the Kapton to a glass slide or silicon wafer.

Chapter 6.3.2 Au-Kapton Failure After Four Weeks

While four point bend testing only occurred at limited intervals, optical inspection and observation of the samples was performed daily. After as few as three weeks, the Au-Kapton samples were starting to show signs of degradation. Optical images were not taken as the saline solution did not allow for good resolution for photographs. However, cracking and wrinkling of the gold was observed visually. Total gold delamination and failure occurred at approximately the four week mark.

As mentioned earlier, de-ionized water was periodically added to the saline solution bath to account for evaporated water. This water addition represented the only mechanical disturbance of the samples during the entire test. It was generally done carefully to avoid pouring selectively on any one sample. However, during the water addition at the four week stage, the small disturbances in the water bath were enough to trigger catastrophic delamination in the samples without adhesion layers. Most of the samples showed partial (at least 50%) degradation, while one sample had complete gold delamination. An optical micrograph of one of the partially failed samples is shown in Figure 6.1 below.

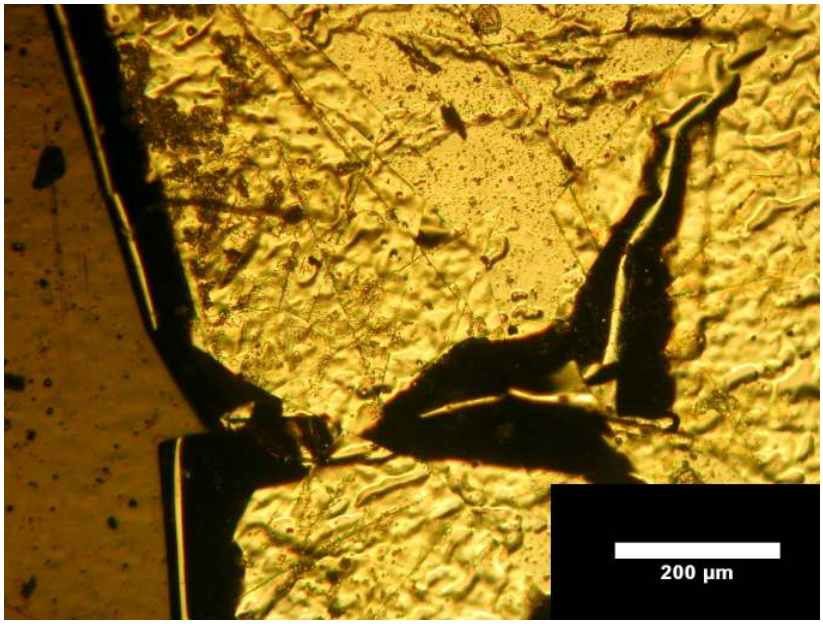

Figure 6.1 Gold film peeling away from Kapton after 4 weeks

In the figure, several interesting details are observable. First, the gold is seen to curl away from the Kapton on the left side of the image. This curling may be due to blister formation and rupture, or it may be due to peeling effects after crack formation. The rather large bulge in the center of the figure does not seem to have any openings, indicating that any space between the gold and the Kapton is not occupied by water from an open crack. It is possible that microcracks exist in the surface which are too small to be seen, but a more likely solution is that water or heavily concentrated ionic solution reached the interface by diffusion through the polymer or along the polymer – metal interface. Furthermore, it is interesting to see a large amount of wrinkles or buckles in many different directions. Implications of this will be discussed shortly.

If the bulges are not simply solution-caused blisters, another possibility is that bulges formed from compressive stresses, as is often seen in thin film failure.[5] However, the gold is sputter deposited in tension, and the swelling of the Kapton should only

increase the tension in the film, meaning that compressive stresses would not be present during the immersion. However, the bulges could have formed after removal from the solution. A reduction in swelling of the Kapton could have compressed the gold if it had achieved equilibrium while in solution. The larger coefficient of thermal expansion for Kapton, along with the tendency to swell when absorbing water, makes this proposed equilibrium unlikely. Indeed, it is more than likely that the Kapton would continuously increase in dimension over time, further straining the interface and weakening the material properties.[6] Studies on polyimide water absorption show that this behavior is common for this class of materials.[7] The continuous uptake of the polyimide explains why the gold eventually fractured catastrophically, as the strain at the interface became too great for the gold to absorb.

If the buckles formed from compression which occurred from sudden removal from the immersive system, it would be analogous to buckle formation in bulge tested gold-Kapton systems, where polymer creep over time allowed relief of the as-deposited tensile stresses in the gold film, and sudden relaxation of the bulge pressure caused a net compression on the gold and ultimately buckle formation observed by McNabb et al.[8] However, McNabb et al. observed a definite directional preference of the buckles in gold-Kapton due to the semi-crystalline nature of the polymer, whereas no directionality is observed in Figure 6.1. Perhaps a more likely solution is that the uneven cracking and sudden delamination of the tensioned gold may have led to a recoil of the undamaged parts of the film, instantly snapping the film back from tension and overcompensating into compression. The interface was clearly already in a degraded state, and the small

compressive forces induced by such a catastrophic failure could have been large enough to cause buckling.

The proposed model of failure in the gold – polyimide system with no adhesion layer is thus tensile cracking from polymer swelling or blister formation, followed by abrupt buckle or wrinkle formation from a catastrophic failure event. In the actual electrodes, such dramatic recoil events are unlikely due to the isolation of every trace from each other and the protective layer of SU-8. However, cracking in the gold is still possible, and probably will remain the main failure mechanism of the electrodes if the interfacial adhesion is not improved via an adhesion layer.

Chapter 6.3.3 Ten Week Specimen Microscopy

Since all of the gold specimens had failed less than halfway into the test, only Au-TiW-Kapton and Au-Cr-Kapton samples were terminated after ten weeks. Optical microscopy was performed on the samples prior to four point bend test specimen preparation. A typical micrograph is shown in Figure 6.2.

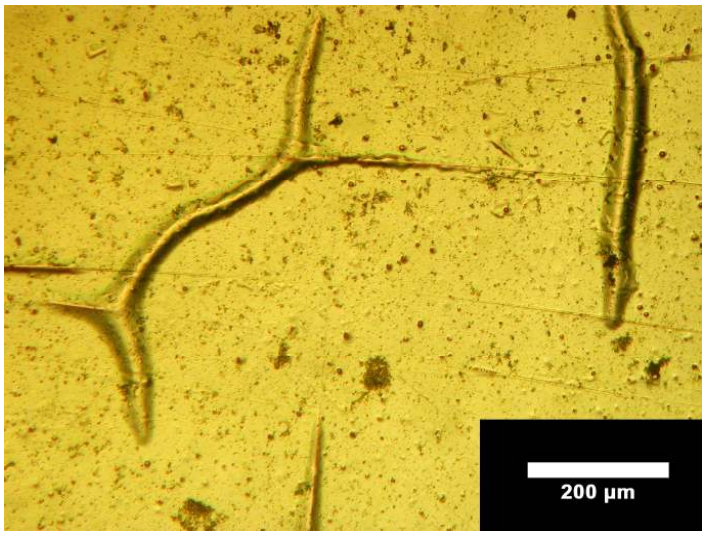

Figure 6.2 Typical surface for Au-Cr-Kapton after immersion

In comparison with Figure 6.1, there are very few if any cracks, and the small ones appear like they could actually be buckles. It is also interesting that there appears to be a preferred buckling direction, vertically in the case of this photo. There may also be a secondary buckling direction, roughly horizontal here. Figure 6.3 shows the preferred buckling direction at the edge of the sample.

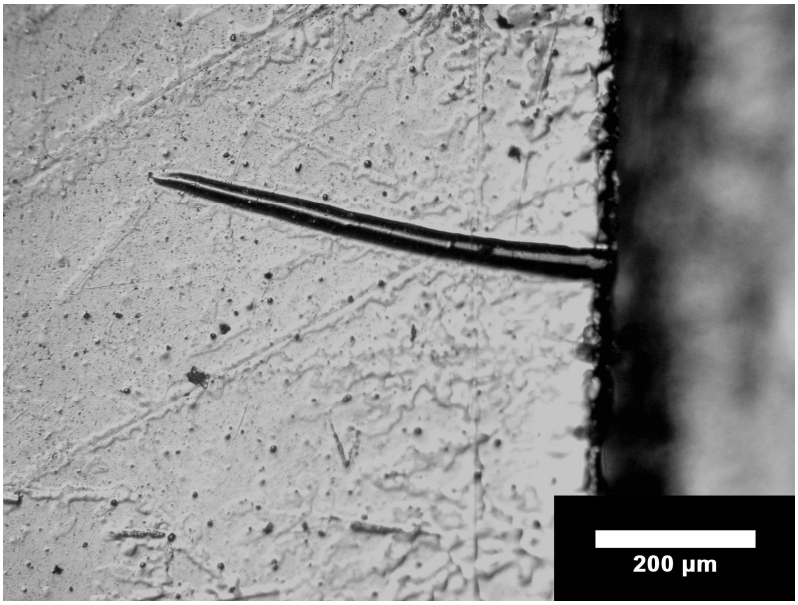

Figure 6.3 Buckle forming perpendicular to edge of sample

This evidence sheds some light onto the damage mechanism present upon removing these samples from the solution. The buckle appears to have been forced from relatively unidirectional contraction of the film. In contrast to Figure 6.1, which shows buckling under anisotropic contraction and cracking failure, Figure 6.3 provides evidence that the buckles do form in some preferential way – in this case, perpendicular to the longitudinal side of the rectangular sample. This unidirectional nature may be explained by the fact that the samples were in slight tension in the longitudanal direction and

contraction in the transverse direction by the tape which affixed them to sample holders in the water bath. It is possible that the contraction was thus greater upon removal in one direction than the other.

It is interesting that the buckles were formed without any cracking and recoil in the sample, as hypothesized in the previous section. It is unlikely that the mere presence of an adhesion layer completely changed the mechanism of failure from cracking to buckling and delamination upon removal from solution. Further study of the buckle formation is necessary to truly reveal the failure mechanism in these samples. However, the most important information obtained from these samples is that they survived the accelerated 10 week test without critical failure.

Chapter 6.4 Four Point Bend Testing Of The Ten Week Specimens

After microscopy, four point bend test specimens were fabricated from all surviving samples. The method used was the same described in Chapter 3, though extra care was taken with these delicate samples. Delamination still occurred in a few of the samples during routine cutting and preparation, but some usable samples were obtained and tested. Figure 6.4 gives a comparison of the typical load-depth curve for immersed samples and their respective normal samples.

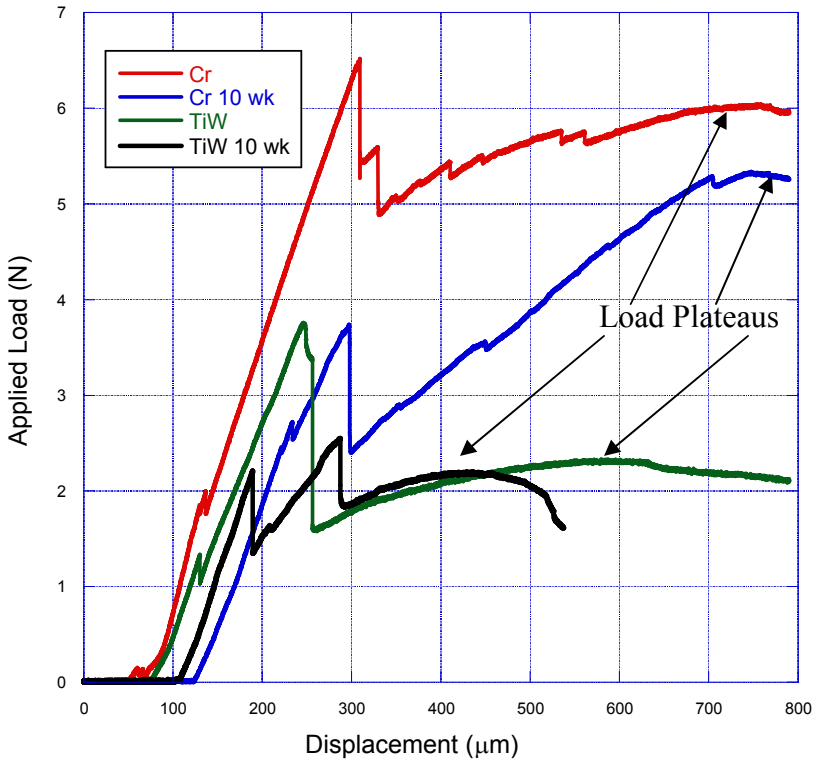

Figure 6.4 Load – displacement curves for 10 week samples compared with non-immersed samples

The graph clearly shows decreases in the horizontal crack propagation plateau after the immersion study, which in turn is evidence of a weaker interface after immersion. Energy values were calculated using Equation 1 from Chapter 2, and the results are given in Table 6.1. The energy values for the non-immersed samples are reproduced from Chapter 5.

Table 6.1 Average interfacial energy values for four point specimens (J/m^2)

	Non-immersed	Immersed for 10 weeks	$p^{(a)}$
TiW	1.8	8.4	0.02
Cr	0.9	3.0	0.05

(a) Welch-Satterthwaite t-test method p-value

The p-values were calculated using the same method as in Chapter 5. The statistical analysis shows that the 10 week immersion process significantly decreased the strength of the metal-polymer interface with at least 95% confidence.

Auger Electron Spectroscopy was performed at Sandia National Laboratories in Livermore, CA, to verify that gold delamination indeed occurred. It was difficult to detect the adhesion layer on either the epoxy or Kapton side of the specimen, and thus it is unwise to make assumptions about the specific chemistry effect of immersion on the adhesion layer properties. However, the combination of AES and four point bend testing confirms that the adhesion layer continues to have an impact on electrode reliability. The differences in relative adhesion decreases between TiW and Cr are interesting in their non-uniformity. While the TiW adhesion weakened by a factor of two, the Cr adhesion weakened by nearly a factor of three. Though futher testing should be done to confirm the data, it seems clear that Au-Cr-Kapton samples were affected by the immersion test to a greater extent than the Au-TiW-Kapton

Chapter 6.5 Conclusions

A ten week immersion test, one which should be an effective simulation of an accelerated version of an implantation test, was performed on three sets of samples: Au-Kapton, Au-TiW-Kapton, and Au-Cr-Kapton. No degredation of any sort was observed after two weeks of immersion. After three weeks, visual cracking was observed in the gold-only samples. After four weeks, the gold-only samples catastrophically failed. The failure mechanism appeared to be critical tensile cracking, followed by multi-directional compressive buckling in the remaining adhered film. Specimens immersed

for ten weeks were removed, rinsed with de-ionized water, and observed under an optical microscope. Micrographs show little to no cracking in the adhesion layer samples, with a small amount of buckles which appear to have preferred orientation. This orientation dependence is attribued to a small anisotropic load placed on the samples during immersion to hold them in place. Four point bend testing shows large decreases in adhesion energy for all samples, though more relatively for the Au-Cr-Kapton specimens. However, the Cr adhesion layer still proves better after 10 weeks than the TiW layer with no immersion. The uneven nature of the interface degradation is interesting, and may lead to further research in the effort to find the best possible adhesion layer.

In conclusion, the TiW and Cr samples appear suitable for at least 10 week implantation, given the accelerated nature of the test and the absence of crack formation over the course of the test. It is possible that fabricated electrodes may last longer than the immersion test length, due to the combination of several degredation factors used in the accelerated test. Considering that further research is needed to assess the biocompatability of a 10nm Cr film, even protected by the gold, it is predicted that Au-Kapton samples with a biocompatable adhesion layer at least as strong as TiW will last 10 weeks or more with few if any failures.

References

[1] J.F. Hetke, K. Najafi, K.D Wise. Flexible Miniature Cables for Long-term Connection to Implantable Sensors. Sensors and Actuators A 21 (1990) 999-1002.

[2] J. Pommersheim, T. Nguyen, Z. Zhang, C.Lin. Cation Diffusion at the Polymer Coating / Metal Interface. Journal of Adhesion Science and Technology 9, 7 (1995) 935-51

[3] B.A. Hollenberg. A MEMS Based Electrode Array For Cortical Surface Potential Recordings. Masters Thesis, Washington State University, December 2005.

[4] M.W. Lane, J.M. Snodgrass, and R.H. Dauskardt. Environmental Effects on Interfacial Adhesion. Microelectronics Reliability 41 (2001) 1615-24.

[5] A.A. Volinsky, N.R. Moody, and W.W. Gerberich. Interfacial toughness measurements for thin films on substrates. Acta Materialia 50 (2002) 441-66

[6] R. DeIasi and J. Russell. Aqueous degradation of polymers. Journal of Applied Polymer Science 15 (1971) 2965-74

[7] W.P. Paplham, R.A. Brown, I.M. Salin, and J.C. Seferis. Absorption of water in polyimide resins and composites. Journal of Applied Polymer Science 57,2 (1994) 133–7

[8] In preparation: P. McNabb, J. Yeager, D. Bahr, and M. Kennedy. Interfacial Fracture Testing of Thin Films on Compliant Substrates. Scripta Materialia

CHAPTER 7

LONG TERM IMPLANTATION IN AWAKE RATS

This chapter describes the chronic implantation of the fabricated electrodes described in Chapter 3. The interfacial toughness measurements reported in Chapters 4 and 5, as well as the fluid immersion experiment from Chapter 6, all culminated in an electrode array suitable for long term implantation. All surgical procedures were performed in accordance with the "Guide for the Care and Use of Laboratory Animals" approved by the Washington State University Animal Care and Use Committee.

Chapter 7.1 Review of Relevant Experimental Procedure

64 channel electrode arrays were fabricated as described in Chapter 3. While the number of working channels was acceptable, the currently available signal processing capabilities limited the number of real-time channel recordings that could be made. As a result, fabricated electrodes were cut with a razor into 6 to 12 channel arrays. Copper wires and silver epoxy were then used to create leads from the top of the electrode array to a custom-fitted skullcap. The individual leads were protected with an epoxy, as illustrated in Figure 7.1

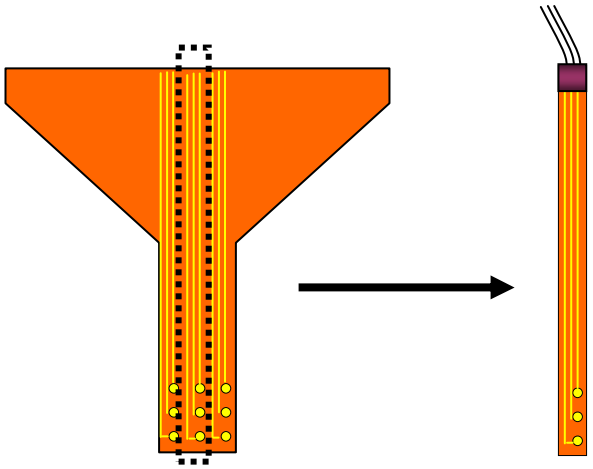

Figure 7.1 Schematic of cutting the full electrode into a strip for implantation

Cut electrodes were implanted in female Sprague-Dawley rats, as shown in Figure 3.7 in Chapter 3. All surgery was performed by Dr. Manuel J. Rojas or Dr. David M. Rector. First, the rats were anesthetized using Isoflurane (5.0%). A small slit (1x5 mm) was created in the skull and the electrode array was inserted between the bone and the dura over the auditory and somatosensory cortex. A stainless steel signal-control screw was implanted over the parietal lobe, while three other screws served as ground references and gave background information on the state of the animal. Penicillin was given at the end of the surgery to combat any bacteria introduced during surgery, while Flunixin was given as an anti-inflammatory agent shortly after the surgery. The rats then were allowed to recover for two to three weeks.

After recovery from surgery, the rats were placed in a 30x30x50cm box and connected to a customized amplifier and data recording system. The connection allowed for free movement inside the box. The auditory cortex was stimulated using speaker clicks for 30 minutes, and the response signals from the rats were filtered between 0.1 Hz and 3.2kHz, then sampled at 10 kHz. The system recorded about 1,200 evoked response

potentials (ERP) per session and the average ERP amplitude was calculated for each gold and screw electrode.

Chapter 7.2 Evoked Responses for Implanted Electrodes

Several Au-TiW-Kapton electrodes were fabricated and implanted in rats for time periods ranging from 50 days to several months (ongoing at the time of this thesis). In addition, Au-Ti-Kapton electrodes have been fabricated and will be implanted as soon as possible. Some electrode responses are presented in this section.

Chapter 7.2.1 Au-Tiw-Kapton Electrode Implanted For 50 Days

A cut electrode was implanted in a female rat for 50 days. Figure 7.2 shows a typical electrode channel responding to neural signals at several time intervals during implantation. The ERP amplitude recorded from the gold electrode was similar in shape and size to the ERP recorded from the control electrode. There was a slight shift in the P1 and N1 latencies due to the differences in the control electrode placement relative to the gold electrode array.

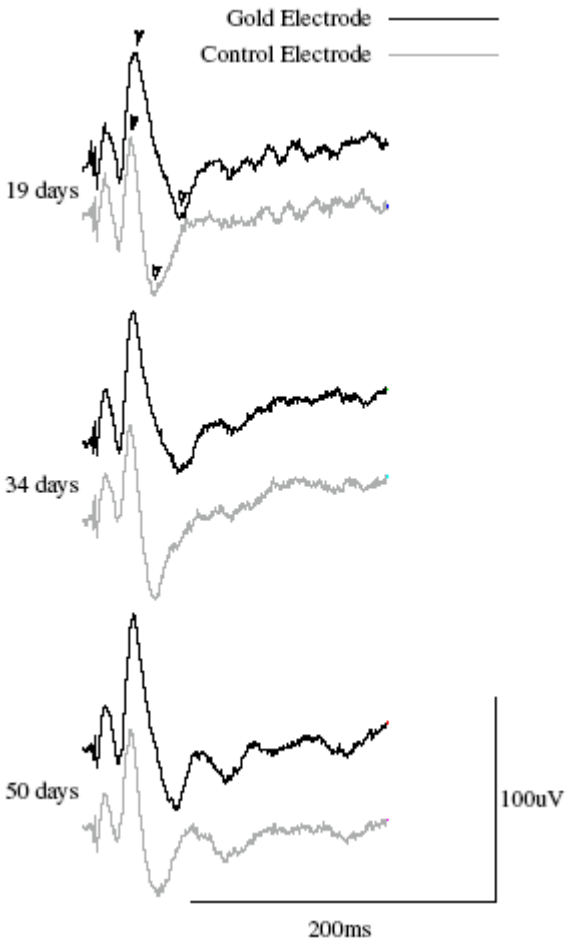

Figure 7.2 Electrode and control screw responses over 50 days. The arrows are to draw attention to the slight shift in the peaks – this is due to small location differences between the gold electrode pad and the screw.

The amplitude of the ERP recorded from the gold electrode appeared to have less deviation (range = 23.630 mV) between recording days than the control electrode (range =45.930 mV) for a period of 50 days. This was a positive result, indicating that the flexible electrode performed at least as well as the metal screw. Derrick J. Phillips, who assisted with surgery and neural recordings, performed a least squares regression calculation for days implanted vs. amplitude proved that the amplitude of the response

did not depend on the number of days implanted for both gold (r = 0.26) and control (r = -0.57). The results of this regression are shown in Figure 7.3. A coincidence calculation found at a 95% confidence level the lines do not statistically differ (F = 1.71)

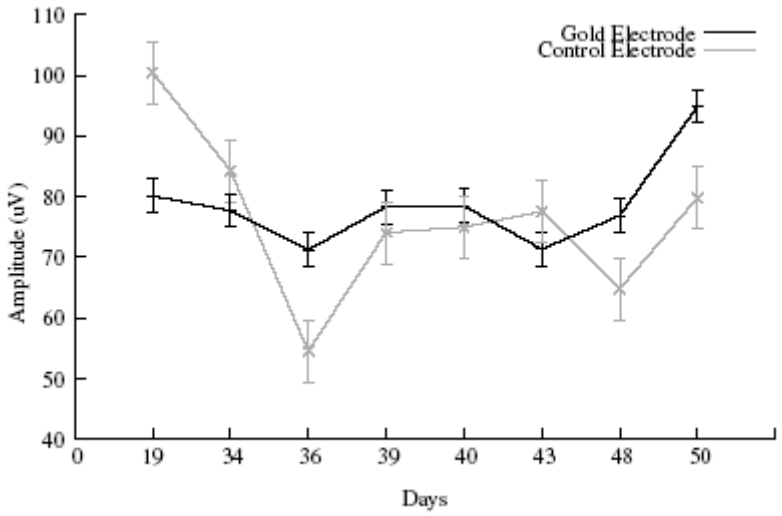

Figure 7.3 The average amplitude plot for the surface evoked responses across time

While at least one channel worked for the entire duration of the test, the principal reason for terminating at 50 days was to examine a channel which had failed. Figure 7.4 shows a control screw and two working channels after 19 days of implantation, and only one working channel after 50 days. The sinusoidal pattern of Channel 4 in Figure 7.4 is

typical of noise from an open circuit.

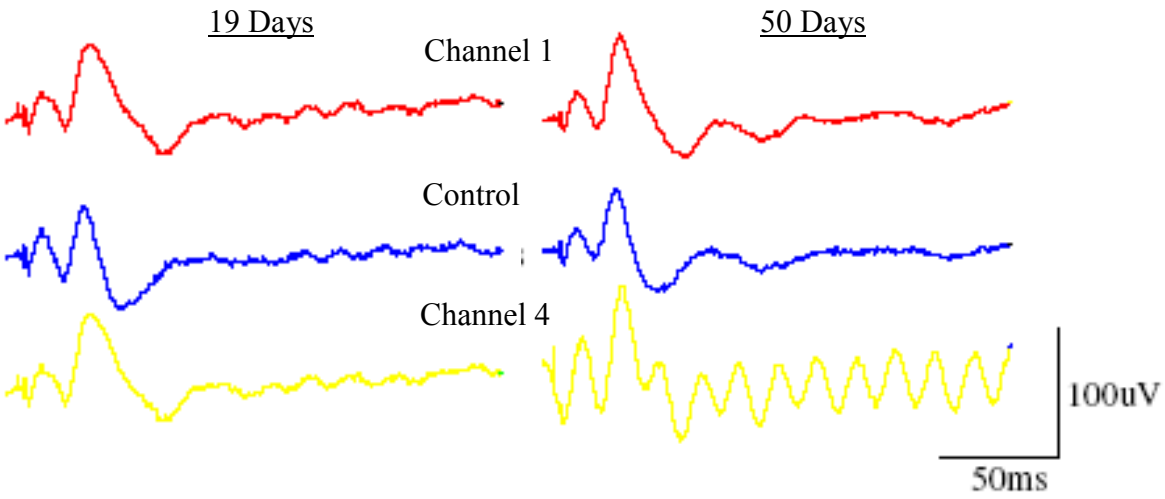

Figure 7.4 Evoked response from both a working and a failed channel

While implanted, it was not possible to determine whether the loss of signal in Channel 4 was due to a failure in the electrode or a shutdown of brain tissue in the local area, so the test was terminated to perform a failure analysis. However, when the sample was cleaned and prepared for optical microscopy, the SU-8 delaminated from the Kapton and peeled the gold off with it. This provided an unexpected opportunity to examine the gold-Kapton interface. Figure 7.5 is an electron micrograph of the SU-8 "substrate" with the gold resting on top. The figure shows a sharp, brittle fracture of the gold, as well as evidence of some sort of film on top of the gold. It is possible that fluid from the brain seeped in between the gold and the Kapton, causing delamination. It is also possible that the fluid seeped in after the gold had already delaminated from some other event. Further research is necessary to determine the exact failure mechanism.

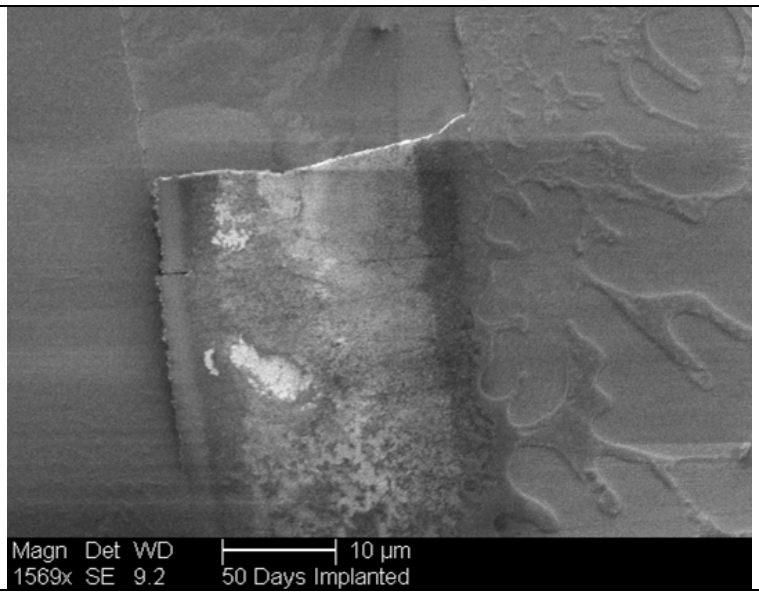

Figure 7.5 Micrograph of gold failure in 50 day specimen

While it is impossible to say at this point whether the gold failures are purely from the implantation environment or from sample preparation, the results presented here still have some significance. No evidence was found of corrosion or worn down gold traces or pads, so at this point it can be said that the failure was probably sudden and critical. Further analysis of implanted electrodes should be undertaken as soon as the tests are terminated in order to gain greater understanding of the failure mechanism.

Chapter 7.2.2 Ongoing Implantation And Results From 80 Days

There are currently several Au-TiW-Kapton electrode arrays implanted in rats. Unlike the previous specimen, these arrays will continue recording until no channels remain functional. One electrode has still provided useful data after 80 days of implantation, and the evoked response is compared to the control screw in Figure 7.6.

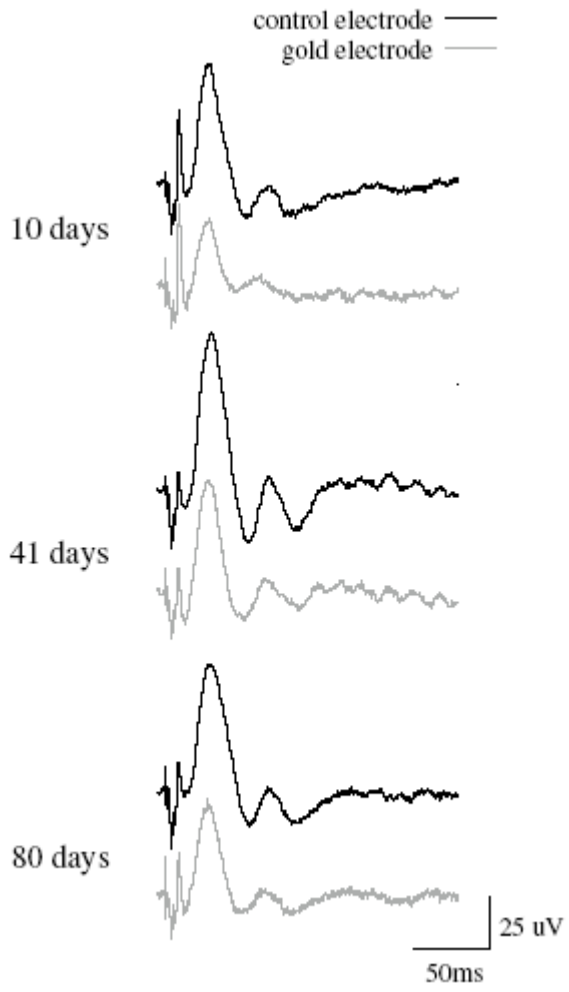

Figure 7.6 Evoked response for an electrode after 80 days

Note that the 80 day specimen has now lasted longer without signs of failure than the Au-TiW-Kapton specimens in the harsh conditions of the accelerated simulated implantation test in Chapter 6. This electrode array has demonstrated good reliability thus far and will remain implanted as long as possible.

Chapter 7.3 Summary and Conclusions

Flexible electrode arrays, consisting of gold on Kapton with a TiW adhesion layer, have been implanted in Sprague-Dawley female rats for up to 80 days with good reliability. The signal from the array shows better consistency than the control screw electrode at least over a period of 80 days, and statistical comparison of the actual evoked responses shows that they are not significantly different. Auditory stimulation has been shown to evoke responses even in awake, moving rats, and the arrays can satisfactorily record such responses. Au-Ti-Kapton electrodes have been fabricated and are in line to be implanted as soon as possible. It is anticipated that these new electrodes will significantly outperform the current batch, based on the improved durability results demonstrated in Chapter 5.

CHAPTER 8

CONCLUSIONS AND RECOMMENDATIONS

This chapter summarizes all of the research performed for this thesis. Some brief remarks will be made concerning the future aims of the project, both from the implantation perspective and the four point bend test mechanics perspective.

Chapter 8.1 Fabrication Improvements to Existing Electrode Design

Hollenberg developed a 64 channel flexible electrode array that was suitable for short term implantation in anesthetized rats.[1] However, only 53 electrode channels on average worked per fabricated array. In addition, the alignment jig for connecting the implanted electrode to a recording system was bulky and therefore unsuitable for awake and moving animals. The array had other minor issues like curling of the device and sharp or jagged edges which could cause trauma in the brain.

Improvements in the clean room microfabrication of the device solved several of these problems. Optimization of the photolithography methods, plasma etching parameters, gold etching processes, and SU-8 cure time led to planar electrode arrays with an average of 60 working channels per device.

A stamping process, using a steel-rule die, proved suitable for removing the arrays from the carrier film after clean room fabrication. The stamped edges were compared to edges cut with a razor and with scissors. Stamping was shown to provide uniform, neat edges comparable to those from the razor, while scissor cut edges were too jagged. An

additional advantage to stamping is that it is a repeatable process, convenient for scaled-up production processing if necessary.

A new gold pattern was designed to accommodate small, lightweight 32 pin connectors for long term implantation. The pin connectors can be precisely aligned under a microscope for perfect connection with the device. The new gold pattern was smaller and more compact than previous designs. The combination of smaller feature sizes and lighter connection proved acceptable in principle for long term implantation.

Chapter 8.2 Improvements to Device Durability

While oxygen plasma etching had been previously shown to improve adhesion of metal to Kapton,[2] the effect had not been quantified for the gold-Kapton electrode array used in this study. The effect of a three minute plasma etch on metal-Kapton interfacial toughness was determined for several different metals by a four point bend testing method. Each metal tested was shown to have a significant increase in adhesion energy due to the plasma etching, with the additional insight that not all metals increased the same amount.

Four point bend testing also was used to characterize the relative toughness of the device with different metal adhesion-promoting layers. While chromium was shown to be the most effective interlayer of the metals considered, titanium and a titanium-tungsten alloy were both shown to be suitable biocompatible layers for improving durability. All adhesion layers tested showed marked improvement from gold-only devices.

Chapter 8.3 Long Term Implantation

An accelerated simulation of implantation testing was conducted on gold-Kapton samples with several different interlayers. While the gold-only samples failed after four weeks, TiW and Cr samples survived the ten week test. The decrease in interfacial toughness due to immersion testing was determined using the four point bend test. Despite the 10 week immersion, all the interlayer specimens maintained device integrity, showing that a conservative prediction of at least 70 days of implantation should be possible considering the accelerated nature of the test.

Several Au-TiW-Kapton electrode arrays were fabricated, cut down to a 6-12 channel size, and implanted in female Sprague-Dawley rats. The arrays recorded meaningful data for at least 80 days, and were still providing data at the time of this thesis.

Chapter 8.4 Recommendations

Several improvements to the current electrode design remain to be made. First, a fully working Au-Ti-Kapton 64 channel array should be tested with the new pattern and connectors for long-term viability. Chrome-glass lithographic masks could be utilized to improve the precision of the pattern, improving the yield of working channels per array. Different methods of attaching the connector to the electrode need to be investigated to determine the overall impact on impedance and therefore signal recording ability. These methods may include gold wire bonding, silver epoxy bonding, or one-dimensional conductive tape.

While oxygen plasma etching was shown to significantly improve adhesion of the gold to the Kapton, the effect of different processing parameters was not investigated. Specifically, the RF power, etching time, and oxygen flow rate all potentially affect the surface chemistry changes of the polyimide. These parameters could be optimized in order to make the most reliable electrode possible.

Titanium and TiW were shown to improve the toughness of the device. However, gold and Kapton were chosen for all sample testing. It would be interesting to see if using another brand of polyimide would have a significant effect on the reliability of the electrode. Similarly, other biocompatible metals could be tested. Platinum-titanium-polyimide electrode arrays are being used elsewhere[3], and four point bend testing could be used to determine whether those materials lead to better device reliability. In addition, greater understanding of the mechanics of four point bend testing on compliant substrates could lead to insights in plastic deformation and fracture behavior in the electrode.

References

[1] B.A. Hollenberg. A MEMS Based Electrode Array For Cortical Surface Potential Recordings. Masters Thesis, Washington State University, December 2005.

[2] S.H. Kim, S.W. Na, N.E. Lee, Y.W. Nam, and Y. Kim. Effect of surface roughness on the adhesion properties of Cu/Cr films on polyimide substrate treated by inductively coupled oxygen plasma. Surface & Coatings Technology 200 (2005) 2072 – 9.

[3] T. Stieglitz and M. Gross. Flexible BIOMEMS with electrode arrangements on front and back side as key component in neural prostheses and biohybrid systems. Sensors and Actuators B 83 (2002) 8-14

APPENDIX A

UNCERTAINTY ANALYSIS

This appendix presents a standard analysis of error and uncertainty in the measured values for this thesis. The discussion in sections A.1 to A.3 is limited to variance of any single measurement of interfacial toughness. Analysis of the difference of measurements for a specific type of specimen has been presented in the main body of the thesis, but will be explained in more detail in section A.4. This appendix emulates the uncertainty analysis from Chapter 2.5 of the Engineering Statistics Handbook:

NIST/SEMATECH e-Handbook of Statistical Methods, http://www.itl.nist.gov/div898/handbook/mpc/section5, July 2008.

A.1 Description of Errors

Errors may be separated into two categories: random error and bias. Random errors may arise due to time effects, material inhomogeneity, or specific conditions of measurement-such as differing operators, instruments, or environment. Time effects should not be important for the bend test results, though the chronic implantation testing and recordings could be affected. However, since the goal of the long-term studies were to assess viability rather than quantitatively determine time-related effects, no analysis of such effects is undertaken here. Material inhomogeneities could arise from epoxy mixing or impurities in the sputtering targets or process. It is assumed here that any impurities present are minor, and thus the amount of error such impurities cause is far less than the measurement uncertainty. All of the bend tests were performed by the same operator on the same instruments to reduce conditional error sources. However, the temperature and humidity of the laboratory certainly differed day-to-day. As with inhomogeneity, the

environmental conditions are assumed to be insignificant, but for a true quantitative analysis the effect of humidity in particular must be evaluated in further research.

Bias errors may arise from uncertainties in instrument calibration, physical constants, or geometrical misalignment. An assessment of these errors is presented in the next section. The analysis is classified as Type B, meaning that variance and error is assumed to have some statistical distribution for each device. A Type A analysis requires rigorous statistical examination, and indeed is necessary for highly accurate measurements. However, a Type A analysis involves numerous measurements with many devices for each sample, and was determined to be outside the scope of this thesis.

A.2 Uncertainty of Measurements

Interfacial toughness calculations from four point bend test measurements have so far been shown to be valid measures of relative effectiveness of various pretreatments for the gold-Kapton system. In order to assess the quantitative ability of the test, it is first necessary to examine the introduction of error from the measuring devices. For the four point bend test, only two devices were necessary: a load cell and a digital Vernier caliper. The caliper was used for all length measurements, while the load cell recorded the load during crack propagation. A linear fit of the load plateau was used to find the precise load value to use in Equation 1, and the potential error of the fit was disregarded as the error is less than the resolution of the load cell. Equation A.1 is a slightly modified version of Equation 1 in Chapter 2, and Table A.1 describes the variables and their errors. The equation is used to calculate G, the crack propagation resistance along the interface,

$$G = \frac{21L^2P^2}{16\bar{E}B^2H^3} \qquad \text{(A.1)}$$

where P is the load during lateral crack propagation, $\bar{E} = E / (1-\nu^2)$, 21 and 16 are geometrical constants, and L, B, and H are geometrical dimensions as described in Figure 2.1 and Table A.1.

Table A.1 Typical values of the variables used in Equation A.1 with their errors.

Variable	Typical Value	Error
Load (P)	0.5-10N	± 0.1-0.25N
Pin Spacing (L)	11.91mm	±0.005mm
Height (H)	0.50 mm	±0.005mm
Width (B)	7.75 mm	±0.005mm
Modulus ($\bar{E}$)	122 GPa	± 10 GPa

The source of error in the modified modulus is due to conflicting literature reports. The elastic modulus of silicon was used for all samples in this thesis, as silicon wafers were used to stiffen the sandwich specimen as described in Chapter 2. However, the relative size of the silicon to the rest of the specimen may not always have been constant due to random errors in epoxy preparation or Kapton inhomogeneity. As noted in section A.1, these errors were not closely examined here, but should be investigated in further studies.

A.3 Propagation of Errors

While the uncertainty in any particular measurement is useful to know, calculations involving multiple measurements must take all uncertainties into account. A particularly useful method of doing this is called the Root Sum Squares (RSS) approach, which is shown in Equation A.2. The standard variation in the calculated value is found

as a function of the standard variations of each of the components. Using Equation A.1 for the example, Equation A.2 is given as

$$s_G = \sqrt{\left(\frac{\partial G}{\partial P}\right)^2 s_P{}^2 + \left(\frac{\partial G}{\partial L}\right)^2 s_L{}^2 + \left(\frac{\partial G}{\partial B}\right)^2 s_B{}^2 + \left(\frac{\partial G}{\partial H}\right)^2 s_H{}^2 + \left(\frac{\partial G}{\partial \overline{E}}\right)^2 s_{\overline{E}}{}^2} \qquad \text{(A.2)}$$

where s is the standard deviation of the component in question, and the partial derivative of G with respect to a given function is given as, for example:

$$\frac{\partial G}{\partial P} = \frac{\partial}{\partial P}(G) = \frac{\partial}{\partial P}\left(\frac{21L^2P^2}{16\overline{E}B^2H^3}\right) = \frac{21L^2(2P)}{16\overline{E}B^2H^3} \qquad \text{(A.3)}$$

Using the standard errors from Table A.1, Equation A.2 and the necessary permutations of Equation A.3, typical standard errors for interfacial toughness are given in Table A.2.

Table A.2 Calculated standard deviations for various adhesion layer energies

Layer	Interfacial Energy (J/m^2)	Deviation, s	% error
Cr	9.48	0.96	10.1
Ti	5.19	0.53	10.2
Ta	3.34	0.34	10.2
TiW	1.69	0.18	10.4

Therefore, it is appropriate to say that the values reported in this thesis are accurate within 10%. While this is an undesirable number for a strict quantitative report, the results are acceptable for relative toughness comparisons. Further statistical evaluation of the four point bend test method for elastic-plastic sandwich specimen would provide a method for minimizing the error and allowing for higher certainty for each measurement.

A.4 Uncertainty Analysis between Specimens

Two statistical methods were used to determine the independence of a particular data series from any other series. The first method, used in the plasma etching study in Chapter 4, is the Wilcoxon – Mann – Whitney rank-sum test. This is a nonparametric test which is generally useful for sample sets without normal distribution or variance. In general, each data point from Set A is given a point for each quantity in Set B which has a lesser value. The same process is run for each point in Set B against Set A, and the summed value of the points is then used to compute a *p* value. This Wilcoxon method was considered appropriate for the plasma etching data set because the exact effect of etching on the Kapton was not well understood. For example, the specific chemistry changes undergone by the Kapton may vary from sample to sample due to minor oxygen flow rate differences, percent area exposed, or other difficult-to-control parameters.

Conversely, adhesion layer sputtering is relatively well understood, and so the distribution of the sample data points may be somewhat more normal. As such, the Welch-Satterthwaite t-test was used to calculate independence for the comparison of adhesion layers and simulated implantation studies. This is a useful test for samples with normal distribution but dissimilar variances and sample sizes. The *t* value and the degrees of freedom for each data set comparison were then used in conjunction with a Student's t-distribution table to find the *p* value.

The application of these two tests was assisted by:

StatSoft Electronics Statistics Textbook,,
http://www.statsoft.com/textbook/stathome.html, July 2008